IOWA STATE UNIVERSITY
Digital Repository

1-1-1969

Impurities in MgO by instrumental neutron activation analysis

Wayne Dennis Romberg
Iowa State University

Recommended Citation

IMPURITIES IN MGO

BY INSTRUMENTAL NEUTRON ACTIVATION ANALYSIS

by

Wayne Dennis Romberg

A Thesis Submitted to the

Graduate Faculty in Partial Fulfillment of

The Requirements for the Degree of

MASTER OF SCIENCE

Major Subject: Nuclear Engineering

Iowa State University
Ames, Iowa

1969

TABLE OF CONTENTS

CHAPTER I.   PURPOSE AND NATURE OF THIS INVESTIGATION

Single crystals of magnesium oxide can accommodate small amounts of impurities in either substitutional or interstitial positions of the crystal lattice. In addition, many transition metal ions have radii near enough to that of magnesium(II) to be accommodated in the lattice. However, the presence of these impurities has a strong influence on many of the physical properties of single crystals such as the ionic conductivity, optical absorption, dielectric loss and high temperature creep. If the impurity has a valence different from the valence of the main constituent of the crystal the effect is particularly strong.

The determination of these impurities at a trace level is therefore very important to the understanding of the properties of magnesium oxide crystals. While other groups may be interested in the optical absorption and dielectric loss, the High Temperature Ceramics Groups of Project Themis is interested in studying the ionic conductivity and high temperature creep mechanisms of single crystals of magnesium oxide. Of primary interest are techniques by which Mn_xO may be diffused into magnesium oxide to alter its creep resistance.

While magnesium oxide samples could be analysed by currently available analytical methods, neutron activation analysis is particularly attractive because of its excellent

sensitivity to most trace impurities, the favorable nuclear characteristics of the MgO matrix and the ability to non-destructively analyse the specimens, "as is", from the high temperature creep test laboratory.

While an activation analysis technique for MgO has been developed (30) it involves destructive wet chemistry. This investigation provides a non-destructive, instrumental technique taking advantage of the recent improvements in gamma detection equipment, namely the high resolution Ge(Li) detector and its associated high stability amplifier. Included is a description of the activation analysis techniques involved, a comparison of the older NaI(Tl) versus the newer Ge(Li) system, a comparison of the qualitative results with those of an emission spectroscopic analysis, and a comparison of the quantitative results with those obtained elsewhere for samples of MgO provided by different manufacturers.

CHAPTER II.   PRINCIPLES OF ACTIVATION ANALYSIS

Activation analysis is a method of elemental analysis based on the formation of radioactive nuclides as a net result of reactions between nuclear particles and the isotopes of the elements of interest. When activated, an isotope may produce a characteristic radiation, typically a gamma ray, which can be used to identify it. Furthermore, the amount of radiation emitted will be in proportion to the amount of the isotope present. Activation may be accomplished through the use of neutrons, protons, deuterons, alpha particles, or high energy photons.

The neutron of thermal energy (2200 m/sec), however, is the most commonly employed particle in activation analysis for the following reasons:

1) Most materials have a large cross section for thermal neutrons.

2) High "thermal" neutron fluxes (10^{13} n/cm^{2}sec or greater) are readily available in many research reactors.

3) Radiative capture is practically the only nuclear reaction that can take place at thermal energy enabling the radioisotopes formed to be isotopic with the target elements. The radiative capture (n, γ) reaction is one in which the target nucleus captures a neutron and gains one unit in atomic mass. The resulting nuclide, a heavier isotope of the activated element, will usually be radioactive and will decay

4

by emitting beta particles and gamma rays.

Since thermal neutrons (2200 m/sec) exist in a nuclear reactor as the result of the random slowing down of the epithermal neutrons born in fission, an irradiation in such a reactor exposes the sample to a spectrum of thermal and epithermal neutrons. A measure of the epithermal to the thermal neutron flux can be determined by activating two foils: one cadmium-covered; the other, bare. The cadmium has a very large cross section for thermal neutrons which cuts off sharply above 0.4 ev, hence the cadmium-covered activation is due almost entirely to neutrons above this energy. The ratio of the bare activation to the cadmium-covered activation is known as the cadmium ratio, and shown by

$$R_{Cd} = \frac{\text{Total flux (thermal plus fast)}}{\text{Epithermal flux}}$$

In some isotopes fast or epithermal neutrons can induce (n,p), (n,α), (n,2n) reactions as illustrated in Fig. 1.

z = number of protons

N = number of neutrons
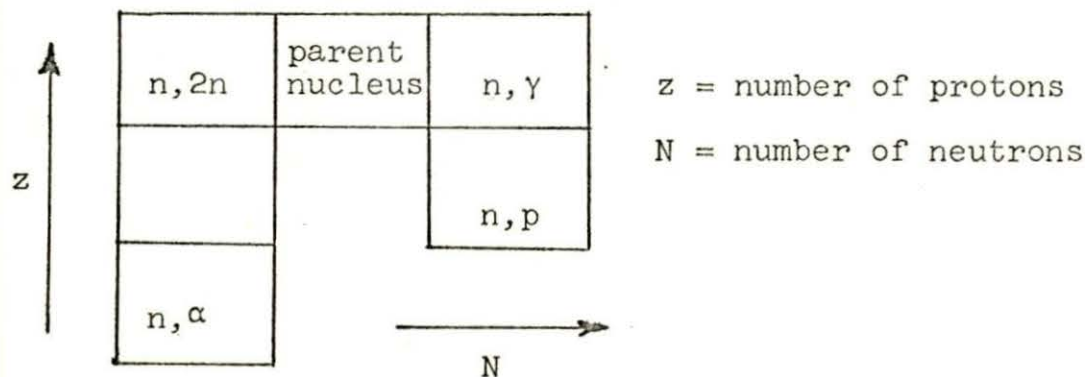
Fig. 1. Fast neutron capture reactions

The rate at which these fast reactions occur is a function
of their energy-dependent cross sections, the specific iso-
tope involved, and the energies of the incident neutrons.

These fast reactions can be either an aid or a hindrance
in activation analysis. They can provide a sensitive way of
analyzing for a nuclide, especially when their fast cross
sections are large and the thermal (n,γ) reaction either
leads to interference with another nuclide or has a small
cross section. Interferences could be in the form of multi-
ple gamma rays at the same energy but from different nuclides
or in the form of high background activity masking the desired
gamma radiation. In either case it would be difficult or
impossible to identify or determine the amount of the nuclide
of interest which is present.

In other instances these fast reactions can be undesir-
able. An irradiation in a "thermal" reactor flux to produce
the (n,γ) reaction can result in fast as well as thermal
reactions. These reactions occur because, as discussed
earlier, a "thermal" reactor flux contains a spectrum of both
thermal and epithermal neutrons. Choosing a reactor irradi-
ation location with a high cadmium ratio can reduce these
fast reactions.

While activation analysis may be based on the detection
of gamma rays, beta particles or X rays; gamma ray spectro-
metry is typically used. Gamma rays may interact with matter

by the Compton, photoelectric, and pair production effects
(18, 21). It is these interactions between photons and the
scintillation (18) or solid state (36) detector that produce
the characteristic gamma ray spectrum of each radionuclide,
a typical example of which is shown in Fig. 2.

In photoelectric absorption the major part of the
energy of the quantum may be absorbed by a bound electron of
an atom. A certain amount of energy is needed to overcome
the binding energy of the atom separating the electron. If
the energy of the incident gamma ray photon exceeds the
binding energy of the K shell, the interaction will be
primarily with that shell. The atom is then left with a
vacancy in that shell which results in the emission of X
rays or Auger electrons. Generally these quanta are immedi-
ately absorbed by a second photoelectric effect, and the
full energy is absorbed within the detector. If this were
the only effect, the full energy of the incident photon
would appear as a sharp photoelectric or full-energy peak.

It is not possible to obtain photoelectric absorption
alone. In the accompanying Compton processes, the incident
photons are scattered by free electrons transferring part
of their energy to the electron. The amount transferred
depends upon the angle of scattering and the energy of the
incident photon. The energy of the scattered photon and
electron are given by the following relationships:
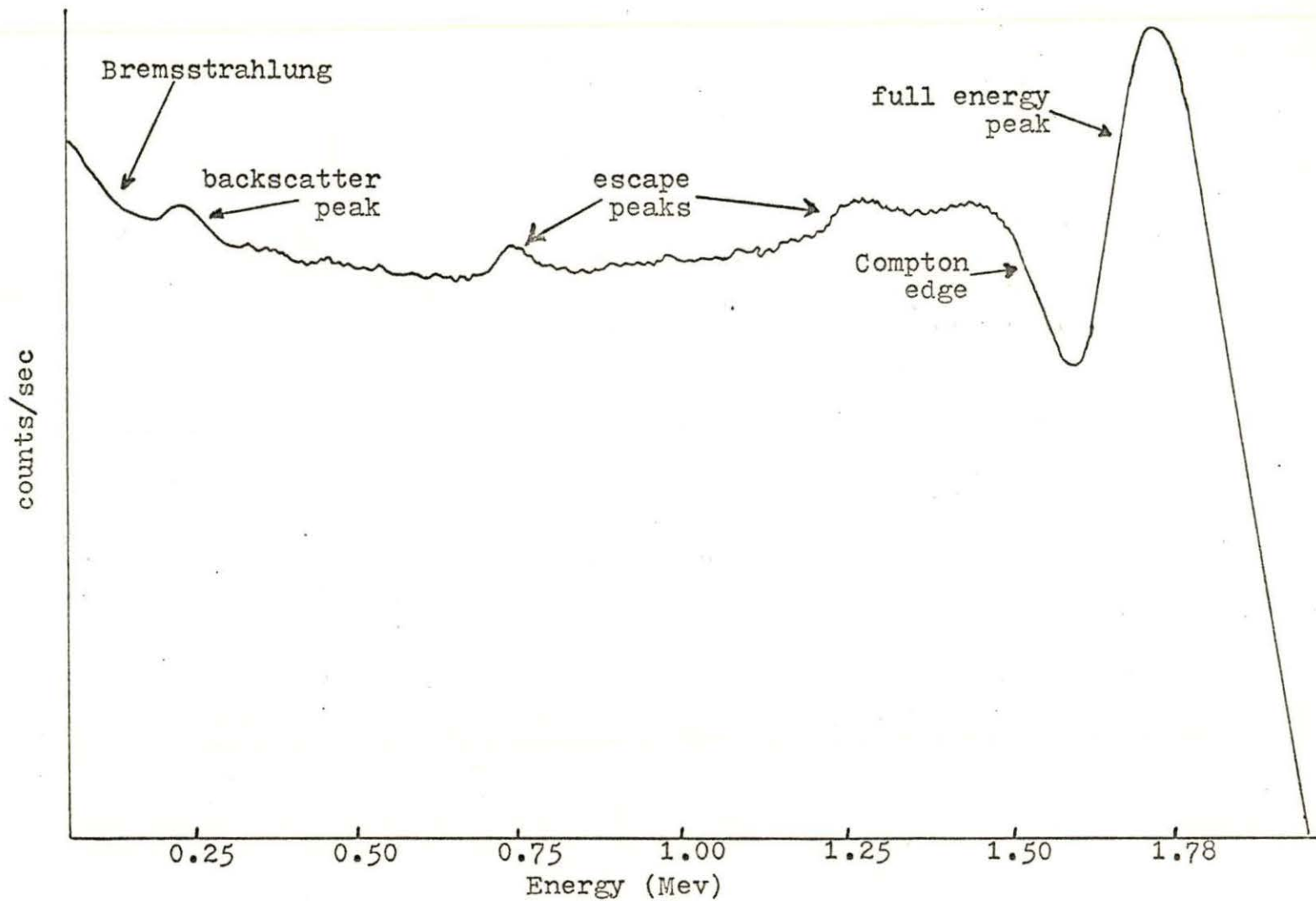
Fig. 2. A typical gamma ray spectrum of 2.3 min Al²⁸

$$E_{\gamma'} = \frac{E_\gamma}{1 + E_0(1-\cos\Theta)} \qquad (1)$$

$$E_e = E_\gamma - \frac{E_\gamma}{1 + E_0(1-\cos\Theta)} \qquad (2)$$

where

E_γ = incident gamma ray energy,

E_e = scattered electron energy,

E_0 = E_γ/mc^2,

Θ = angle between the direction of the primary and
scattered photons.

These relationships show that a Compton electron energy
spectrum will result extending from zero energy at $\Theta = 0^o$
to a maximum energy, at $\Theta = 180^o$. This maximum energy can
be seen on the typical spectrum in Fig. 2 as the Compton
edge. Often the scattered photon will undergo an immediate
photoelectric absorption so that the sum of it plus the
Compton scattered electron will produce a full-energy peak.

If the incident photon has energy in excess of the rest
mass of a positron-electron pair (1.02 Mev), then pair pro-
duction is possible. Upon interaction, which must occur
within the coulomb field of the nucleus, the incident photon
loses 1.02 Mev of energy and a positron-electron pair is
created. The positron combines readily with any available
electron producing two 0.51 Mev annihilation photons. If
both of these photons escape from the detector, the incident

photon appears in the spectrum as an "escape" peak at an energy 1.02 Mev below the actual energy. Similarly if only one annihilation photon escapes, an escape peak 0.51 Mev below the actual energy will be observed (See Fig. 2).

The total probability of detecting a gamma ray is the sum of the probabilities for the photoelectric, Compton, and pair-production processes. At energies up to 0.5 Mev the photoelectric process is most probable. At energies between this and approximately 2 Mev the Compton process is most probable, and above this the pair production process becomes dominant.

Although all parts of the spectrum are characteristic of a particular energy gamma ray, only the full-energy peak areas are normally used to identify and measure a particular radionuclide.

Typically, the spectrum of interest is made up of several component spectra so that the full-energy peaks stand on the background and on the Compton continuum of not only their own spectrum, but on those of others as well. In spite of this, methods can be used to determine the actuall full-energy peak areas. The Covell method[5] consists of locating the full-energy peak center and including all the counts within ∆E on

either side of it. The background is approximated by a
straight line connecting the two ΔE points on the full-energy
peak as shown in Fig. 3.
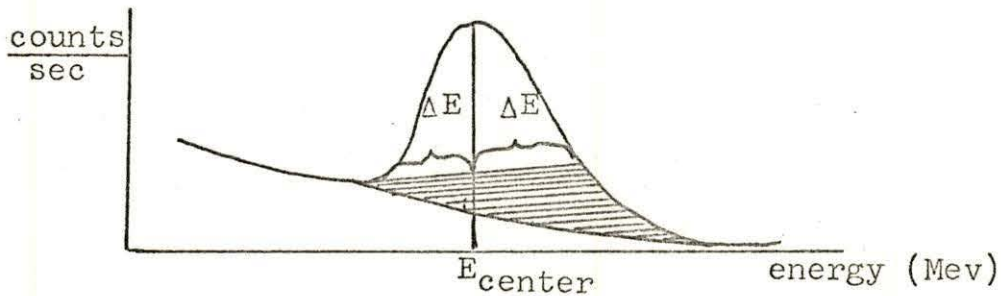
Fig. 3. Full-energy peak area determination by Covell
method

A second method (30) consists of summing the area above a
straight line connecting the feet of the full-energy peak
as shown in Fig. 4.
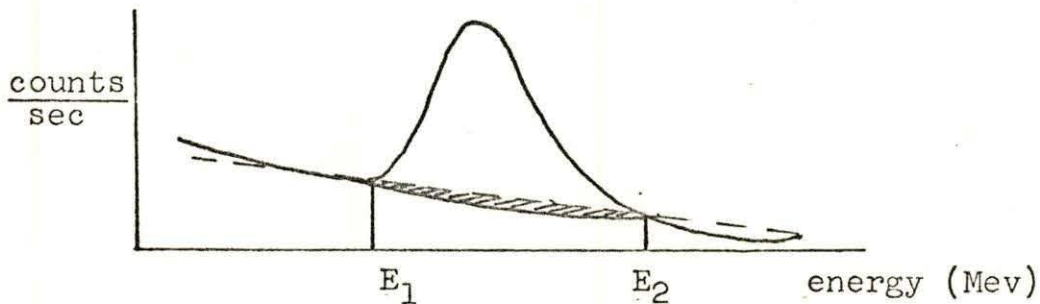
Fig. 4. Area determination by subtraction of background
under full-energy peak feet

Both of these methods result in a systematic error (shaded
areas in Fig. 3 and 4) which is approximately equal for each

sample and may be cancelled out in the comparitor calculations to be discussed later. If the ratio of peak height to background is the same, then the comparison method will work, but if not, it will not because different fractions of peak areas will be removed and the error in background determinations will have different effects on the two spectra.

Because gamma ray emission and detection are statistical phenomena, a spectrum of raw data that should plot as a smooth curve usually does not. Smoothing techniques which can reduce statistical deviations often make both full-energy peak energy and area determination easier and more accurate. To further enhance accuracy, the full-energy peak may be fitted with a gaussian using a least squares technique (18), and its area may be computed from the fitted height and width. Since the calculations involved are tedious, they are usually done with a computer (Appendix A).

Utilization of the nuclear properties of an element rather than the atomic or chemical properties is the principal difference between activation analysis and other analytical techniques. It has two major advantages: First is its extreme sensitivity to most elements. Second, it need not destroy or, in most cases, even alter the sample analyzed. In general, activation analysis, with a sensitivity as high as 10 ppb, ranks slightly below spectrometry and mass spectrometry techniques for qualitative analysis. However, it is superior in quantitative accuracy.

The principal disadvantage is the high cost associated with the necessary facilities, including the sophisticated multichannel analyzer, detector counting cave, and irradiation facilities. In addition, because of the radioactivity involved, trained Health Physics personnel are required.

The activation and decay phenomena upon which neutron activation analysis is based can be explained through the use of mathematical equations. These equations are developed in detail by various authors, including Koch (24) and Friedlander, Kennedy, and Miller (15).

During an irradiation the rate of formation of a particular activation product, R_F, is given by the following equation:

$$R_F = \emptyset n \sigma = \frac{\emptyset m N_0 f \sigma}{A_W} \tag{3}$$

in which

n = the number of target atoms,

$\emptyset$ = the neutron flux ($n/cm^2 sec$),

m = the mass of the target element under consideration (gm),

A_W = the atomic weight of the element under consideration (gm/gm atom),

f = the fractional isotopic abundance of the nuclide,

N_0 = Avagadro's number (atoms/gm atom),

σ = the reaction cross section (cm^2/nuclide).

The rate of decay of this activation product at any given time is given by

$$R_D = \lambda N \tag{4}$$

in which

N = the number of atoms of the activation product present,

λ = the decay constant of the nuclide (sec^{-1}).

The overall rate of formation of the product nuclide during irradiation is given by

$$\frac{dN}{dT} = R_F - R_D = \frac{mN_0 f \sigma \phi}{A_W} - \lambda N \tag{5}$$

The disintegration rate of the activation product at a given time after the end of the irradiation is given by integrating Equation 5.

$$D(sec^{-1}) = \frac{mN_0 f \sigma \phi (1-e^{-\lambda t_i}) e^{-\lambda t_d}}{A_W} \tag{6}$$

in which

t_i = the duration of the irradiation in sec,

t_d = the elapsed time between the end of the irradiation and the time of the count in sec.

For sufficiently long irradiations the $e^{-\lambda t_i}$ term approaches

zero and the disintegration rate approaches a maximum.

$$D^\infty = \frac{mN_0 f\sigma\phi}{A_W} \qquad (7)$$

Therefore Equation 6 becomes

$$D(t) = D^\infty (1-e^{-\lambda t_i})e^{-\lambda t_d} \qquad (8)$$

where

$$(1-e^{-\lambda t_i}) = \text{the saturation factor.}$$

This saturation factor may be plotted as shown in Fig. 5.
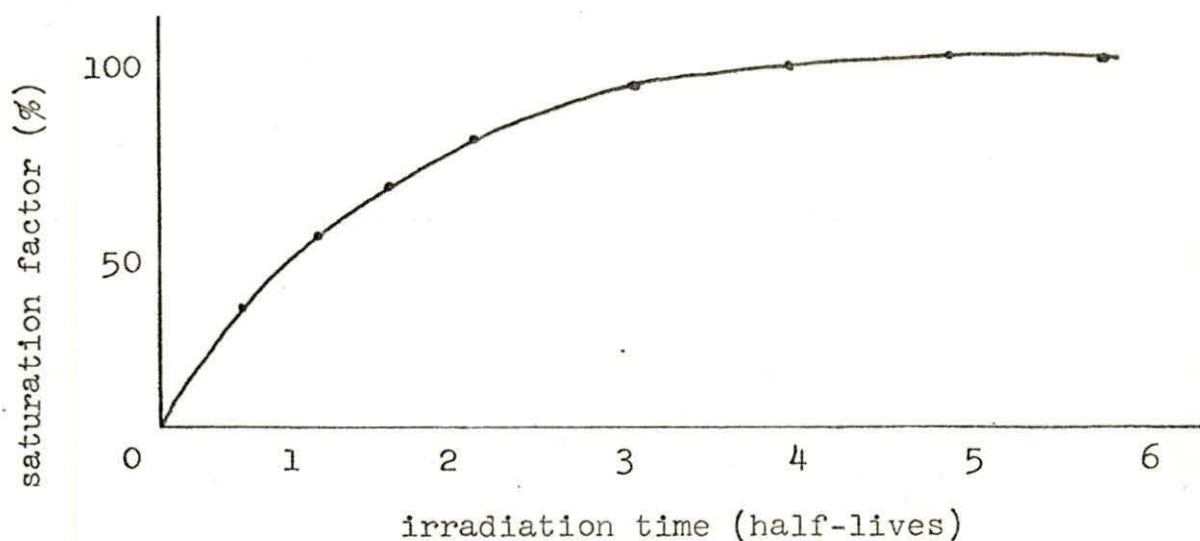
Fig. 5. Saturation factor versus irradiation time

Note that for the first 0.5 half-lives the increase in the saturation factor is approximately linear. Thereafter, it tends to level off until it approaches saturation at approximately six half-lives.

If the sample is allowed to decay for a time t_d sec

and is then counted for t_c sec by a detection system of efficiency δ, the number of counts recorded can be found by integrating Equation 6 over the counting period and multiplying it by both the efficiency and a source-to-detector geometry factor Θ.

$$C = \Theta \delta D^\infty (1-e^{\lambda t_i})e^{-\lambda t_d}\frac{(1-e^{-\lambda t_c})}{\lambda} \tag{9}$$

Here, C is the number of counts recorded which typically, in gamma ray spectrometry, is proportional to the full energy peak area by a peak-to-total ratio. Equation 7 is used for D^∞, and a peak-to-total ratio P is applied, Equation 9 may be written

$$A = \frac{\sigma P\Theta \delta m N_0 f\emptyset (1-e^{-\lambda t_i})e^{-\lambda t_d}}{A_w}\frac{(1-e^{-\lambda t_c})}{\lambda} \tag{10}$$

where

A = full-energy peak area.

Equation 10 may be rearranged into the following convenient form for calculating the sensitivity for detection of an element under a specified set of irradiation and detection conditions.

$$m = \frac{A_{min}\lambda A_w e^{\lambda t_d}}{\emptyset P\Theta \delta N_0 f\sigma (1-e^{-\lambda t_i})(1-e^{-\lambda t_c})} \tag{11}$$

in which

    m   = mass of element (gm),

    A_{min} = minimum full-energy peak area consistent with

          acceptable counting statistics.

The other terms may be inferred from earlier definitions.

Counting statistics are based on the random statistical process of gamma ray emission. The accuracy of a count or full-energy peak area may be given by $A \pm \sigma$ where σ is the standard deviation.

$$\sigma = \sqrt{A} \tag{12}$$

While it is obvious that the accuracy improves with the number of counts accumulated, a longer counting interval may not be the answer. When the comparison method of analysis is used, two samples must be counted before the activity dies.

For the purpose of this study, the maximum counting interval was one-half of the half-life of the activity of the nuclide of interest. If this interval was not sufficient to give a standard deviation less than 5% of the count, i.e., an accumulated count of 400 above background, a higher integrated flux was used to increase the count rate.

Neutron activation analysis may be carried out by either the absolute method or by a comparitor method. The absolute method using Equation 11 requires an accurate knowledge of the detector efficiency, the counting geometry factor, the

peak-to-total ratio, and the absolute disintegration rate.
The disintegration rate in turn requires accurate information
about the neutron flux, the activation cross section of the
target nuclide, and the half-life of the radionuclide pro-
duced.

This method is little used because the measurement of
the actual neutron flux is rather difficult, and the acti-
vation cross sections for most nuclides are not known to a
suitable precision. Furthermore, Equations 6 and 8 assume
that the neutron flux is constant throughout the sample
matrix. This may not be true, especially in a matrix where
nuclides with high neutron absorption cross sections are
present. These nuclides may attenuate the neutron flux
within the matrix causing the inner atoms to experience a
smaller flux than those on the surface. This self-shielding
effect is related to the sample's geometry. This self-
shielding problem may be minimized by reducing the size of
the sample, and while it can be determined by semi-empirical
calculations (35), it must usually be determined experi-
mentally.

The above problems are usually overcome by using the
comparitor method of activation analysis. The comparitor
method does not require either an accurate knowledge of
the neutron flux or the activation cross section. Instead,
a standard or set of standards is irradiated simultaneously

with the sample and is counted under the same conditions.
Using only the counts in the full-energy peak and correcting
for a slight difference in decay-time plus any difference
in counting time, most of the terms in Equation 10 cancel,
and the specific full-energy peak area of the activity of
interest in the standard is equal to the specific full-
energy peak area of the activity in the unknown.

$$\frac{A_S}{m_S} = \frac{A_u}{m_u} \tag{13}$$

The above relationship implicitly assumes that the neutron
flux experienced by both the sample and the standard is the
same. To insure that a flux gradient does not expose the
unknown and standard to different dose rates, they should be
placed in close proximity of one another, preferably along
an equiflux line. In regions where the flux gradient is
steep, it may be necessary to rotate the samples about one
another during irradiation to insure equal exposures. In
the case of a matrix that exhibits considerable self-shielding,
the comparator standard should ideally have a matrix of the
same size and composition as that of the sample (31).

The precision of the m_u determination can be found by
applying the propagation of errors theory (31) to Equation
10 for both the sample and the unknown.

$$\frac{m_u}{m_s} = \frac{\sigma P_s A_u \Theta_s \delta_s m_s N_O f_s \varnothing_s S_s (1-e^{-\lambda_s t_{is}}) e^{-\lambda_s t_{ds}}(1-e^{-\lambda_s t_{cs}})}{\sigma P_u A_s \Theta_u \delta_u N_O f_u \varnothing_u S_u (1-e^{-\lambda_u t_{iu}}) e^{-\lambda_u t_{du}}(1-e^{-\lambda_u t_{cu}})}$$

(14)

Certain of these terms are by definition common to both the sample and unknown. Among these are Avagadro's number, the detector efficiency, the peak-to-total ratio, the isotopic abundance, the half-life, the irradiation time, and the cross section. When these are canceled, Equation 14 becomes

$$m_u = \frac{f_s A_u \Theta_s m_s \varnothing_s S_s e^{-\lambda_s t_{ds}}(1-e^{-\lambda_s t_{cs}})}{A_s \Theta_u f_u \varnothing_u S_u e^{-\lambda_u t_{du}}(1-e^{-\lambda_u t_{cu}})}$$

(15)

Each term on the right hand side of Equation 15 may be expressed as a measurement, weight, or count $\pm$ an uncertainty. For example, the mass of the standard may be expressed as $m_s \pm \Delta m_s$ where the uncertainty Δm_s may be defined as one half the smallest division of the balance. Applying propagation of errors theory to Equation 15 results in the following equation:

$$m_u \pm \Delta m_u = m_s A_R \Theta_R \varnothing_R S_R D_R C_R \left[1 \pm \sqrt{\left(\frac{\Delta m_s}{m_s}\right)^2 + \left(\frac{\Delta A_R}{A_R}\right)^2 + \left(\frac{\Delta \Theta_R}{\Theta_R}\right)^2} \right.$$
$$\left. \overline{+ \left(\frac{\Delta \varnothing_R}{\varnothing_R}\right)^2 + \left(\frac{\Delta S_R}{S_R}\right)^2 + \left(\frac{\Delta D_R}{D_R}\right)^2 + \left(\frac{\Delta C_R}{C_R}\right)^2} \right]$$

(16)

in which

the full-energy peak ratio,

$$A_R \overset{+}{-} \Delta A_R = \frac{A_u}{A_s} \div \frac{A_u}{A_s} \sqrt{\left(\frac{\Delta A_u}{A_u}\right)^2 + \left(\frac{\Delta A_s}{A_s}\right)^2} \tag{17}$$

the counting geometry ratio,

$$\Theta_R \overset{+}{-} \Delta\Theta_R = \frac{\Theta_s}{\Theta_u} \overset{+}{-} \frac{\Theta_s}{\Theta_u} \sqrt{\left(\frac{\Delta\Theta_s}{\Theta_s}\right)^2 + \left(\frac{\Delta\Theta_u}{\Theta_u}\right)^2} \tag{18}$$

the flux ratio,

$$\phi_R \overset{+}{-} \Delta\phi_R = \frac{\phi_s}{\phi_u} \overset{+}{-} \frac{\phi_s}{\phi_u} \sqrt{\left(\frac{\Delta\phi_s}{\phi_s}\right)^2 + \left(\frac{\Delta\phi_u}{\phi_u}\right)^2} \tag{19}$$

the self-shielding ratio,

$$S_R \overset{+}{-} \Delta S_R = \frac{S_s}{S_u} \overset{+}{-} \frac{S_s}{S_u} \sqrt{\left(\frac{\Delta S_s}{S_s}\right)^2 + \left(\frac{\Delta S_u}{S_u}\right)^2} \tag{20}$$

the decay ratio,

$$D_R \overset{+}{-} \Delta D_R = \frac{e^{-\lambda t_{d_s}}}{e^{-\lambda t_{d_u}}} \left[1 \overset{+}{-} \sqrt{(\lambda \Delta t_{d_s})^2 + (t_{d_s}\Delta\lambda)^2} \right.$$
$$\left. \overline{+ (\lambda\Delta t_{d_u})^2 + (t_{d_u}\Delta\lambda)^2} \right] \tag{21}$$

and the counting ratio,

$$C_R \overset{+}{-} C_R = \frac{(1-e^{-\lambda t_{c_s}})}{(1-e^{-\lambda t_{c_u}})} \left[1 \overset{+}{-} \sqrt{\left(\frac{e^{-\lambda t_{c_s}}}{1-e^{-\lambda t_{c_s}}}\right)^2 (t_{c_s}\Delta\lambda_s)^2} \right.$$
$$\left. \overline{+ (\lambda_s\Delta t_{s_c})^2 + \left(\frac{e^{-\lambda t_{c_u}}}{1-e^{-\lambda t_{c_u}}}\right)^2 (t_{c_u}\Delta\lambda_u)^2 + (\lambda_u\Delta t_{c_u})^2} \right] \tag{22}$$

The meanings of other symbols may be inferred from past definitions.

Activation analysis can be performed either destructively in a "hot" laboratory or nondestructively by strictly instrumental techniques. The nondestructive instrumental techniques were chosen.

Instrumental activation analysis relies on being able to resolve the induced activity of the sought element from all other activities in the matrix. It was made effective by the advent of high resolution Ge(Li) detectors. While the detection efficiency of Ge(Li) detectors is lower than that of the older Na(I) detectors, the resolution is so much better (3.3 Kev at 1333 Kev versus 4.8% (FWHM) for Na(I) detectors) that even a complex spectrum may be resolved into its component elements by gamma spectrometry. There are cases in which the characteristic gamma radiation from a nuclide may be masked by identical gammas from another nuclide or group of nuclides. In these cases judicious use of their different half-lives can usually separate them, or one or more of the interferences may be identified allowing its spectrum to be mathematically or mechanically stripped away from the composite spectrum.

CHAPTER III. EXPERIMENTAL FACILITIES AND EQUIPMENT

Irradiation Facilities

The preliminary irradiations were obtained in the Iowa
State University Training Reactor (UTR-10). This is a
heterogenous, tank-type reactor which is water-cooled and
moderated with light water and graphite. The total U^{235}
content of the core is 3 kg enriched to 90%. A pneumatic
rabbit tube which terminates against one of the two core
tanks permits convenient access to the high neutron flux
region during operation. This reactor can at maximum power
provide a flux of approximately 7.0×10^{10} n/cm^2sec. The
cadmium ratio at this location is approximately 5.0.[1]

Later in the investigation when a higher flux and
cadmium ratio were deemed necessary, samples were irradiated
at the Ames Laboratory Research Reactor (ALRR). This is a
5 mw tank-type reactor cooled and moderated with heavy water
and fueled with elements of 93% enriched U^{235} dispersed in
and clad with aluminum. The reactor core assembly consists
primarily of the fuel elements within a tank filled with
heavy water which, in turn, is surrounded by a stainless
steel thermal shield within a tank filled with light water.
A total of 35 experimental facilities, including radiation

---

[1]Danofsky, Richard, Iowa State University, Ames, Iowa.
Flux and cadmium ratio measurements of UTR-10 reactor.
Private communication. 1969.

ports, beam tubes, vertical thimbles, rabbit tube, and a thermal column penetrate the concrete shielding to permit access to the reactor core for irradiation. The facilities used in this investigation are shown in Table 1.

Table 1. Specifications of ALRR facilities used to irradiate MgO samples

Description	Designation	Flux	Cadmium ratio
Rabbit tube	R-3	3.4×10^{13} n/cm^{2}sec	approx. 20
Rabbit tube	R-5	3×10^{13} n/cm^{2}sec	approx. 20
Rabbit tube	R-6	8×10^{12} n/cm^{2}sec	approx. 20
End of thermal column	TV1	6×10^{10} n/cm^{2}sec	approx. 1000

The rabbit tubes pass tangentially to the reactor core making the flux gradient along the length of a rabbit approximately zero but producing a slightly negative gradient across the diameter of the rabbit.

To facilitate the handling of samples with short half-lives, the rabbit tubes R-3 or R-6 above can deliver the sample to a receiving room while simultaneously triggering a timer. The receiving room is in the vicinity of the room containing the gamma ray spectrometer system.

Gamma-Spectrometer System

Radioactivity measurements in this study were done with two gamma ray spectrometer systems. A short half-life qualitative study was done with an Ames Lab Ge(Li) spectrometer system consisting of a Radiation Instrument Development Laboratory (RIDL) transistorized 1600 channel analyzer counting from a Nuclear Diode Model LGC-3.5X Ge(Li) detector. The detector, which is trapezoidal, has an active area of 11 cm^2. Its peak efficiency relative to NaI is 3.5% while the resolution is 3.48 Kev for the Co 1.33 Mev photon.

Analyzer system

Most of the radioactivity measurements were done on the Nuclear Data 2200 multichannel analyzer system shown in Fig. 6, 7, 8, 9, and 10. This system consists of a 4098 channel analog-to-digital convertor, 1024 channel memory, a cathode ray tube display, a tape transport for rapid storage of data, a data/reduce integrate unit, a Teletype typewriter with a paper punch, and the associated control circuitry for automatic or manual operation of the system.

Counting was done in a Heath type (18) shield or cave as illustrated in Fig. 7, 9, and 10. The shield is constructed of lead 4 in. thick and has inside dimensions of 32 in. x 32 in. x 32 in. Its inside surface is covered with 0.30 in. of cadmium which in turn is covered with 0.015 in. of copper. The lead acts to shield the detector from extra-

H.V. Power
Supply

Multichannel Analyzer
Nuclear Data 1024

Det. I
NaI(Tl)
Photomult.

Pre Amp & Amp
Nuclear Data
PAD 520

Pre Amp
ORTEC
Model 118A

Amp
ORTEC
Model 435

Det. II
Ge(Li)
ORTEC 8201-0335

H.V. Power
Supply

Analog to
Digital
Convertor

CRT
Display

Magnetic Tape
Transport and
Reduce/Integrate
Unit N.D.

Master
Control

Memory

Output Teletype
and Paper Tape
Punch

Magnetic Tape
to Card
Punch Using
Program PRESTO

Paper Tape to
Magnetic Tape
Convertor

IBM 47
Paper Tape
to Card Punch

IBM 360/65 Computer
ICPEAX plots spectra, labels peak energies, and
computes peak areas

Fig. 6.   Schematic of detection, counting, and data handling equipment

Fig. 6. Schematic of detection, counting, and data handling equipment
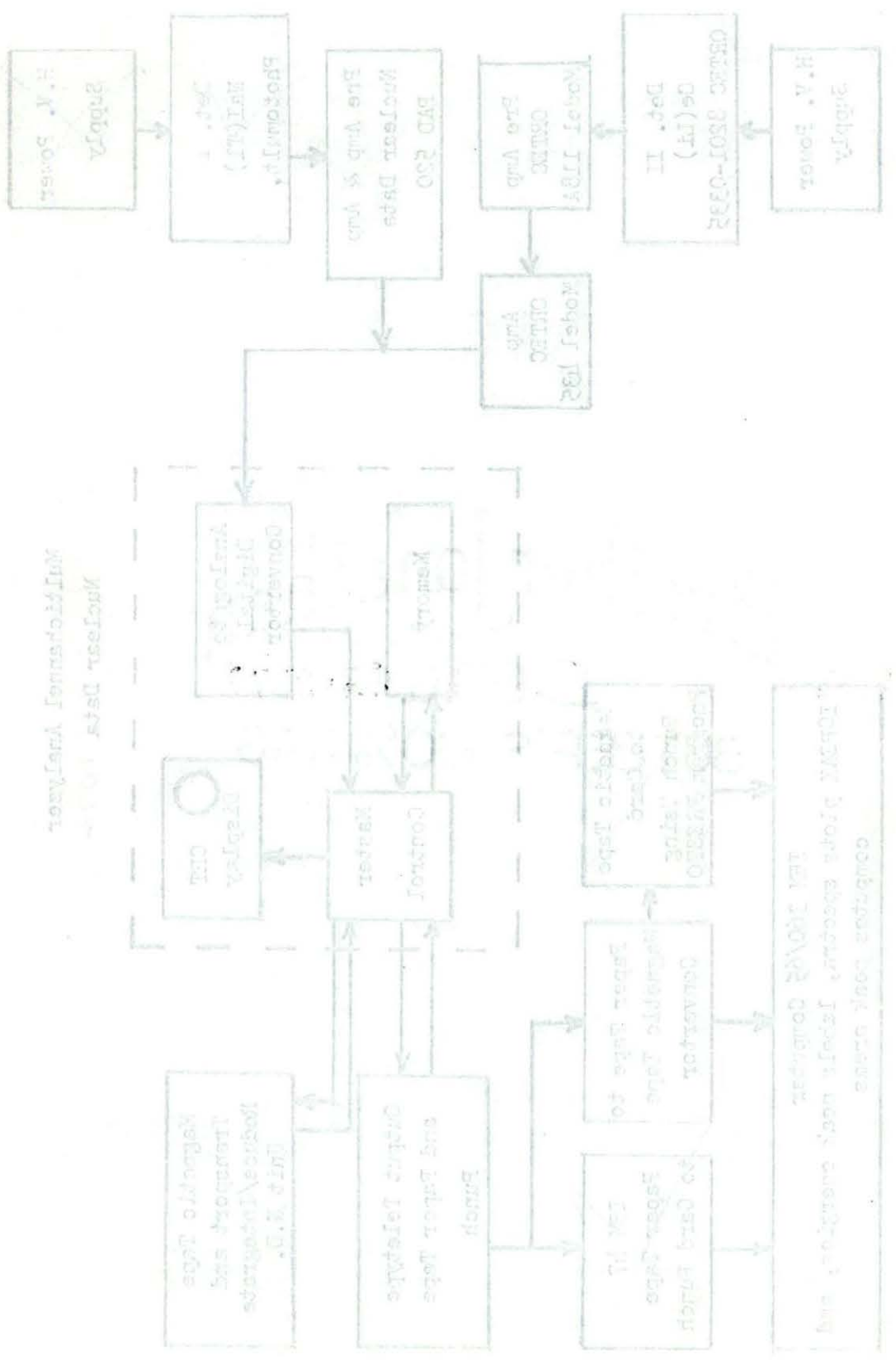
Fig. 7. Gamma ray spectrometer system

Fig. 8. Analyzer system
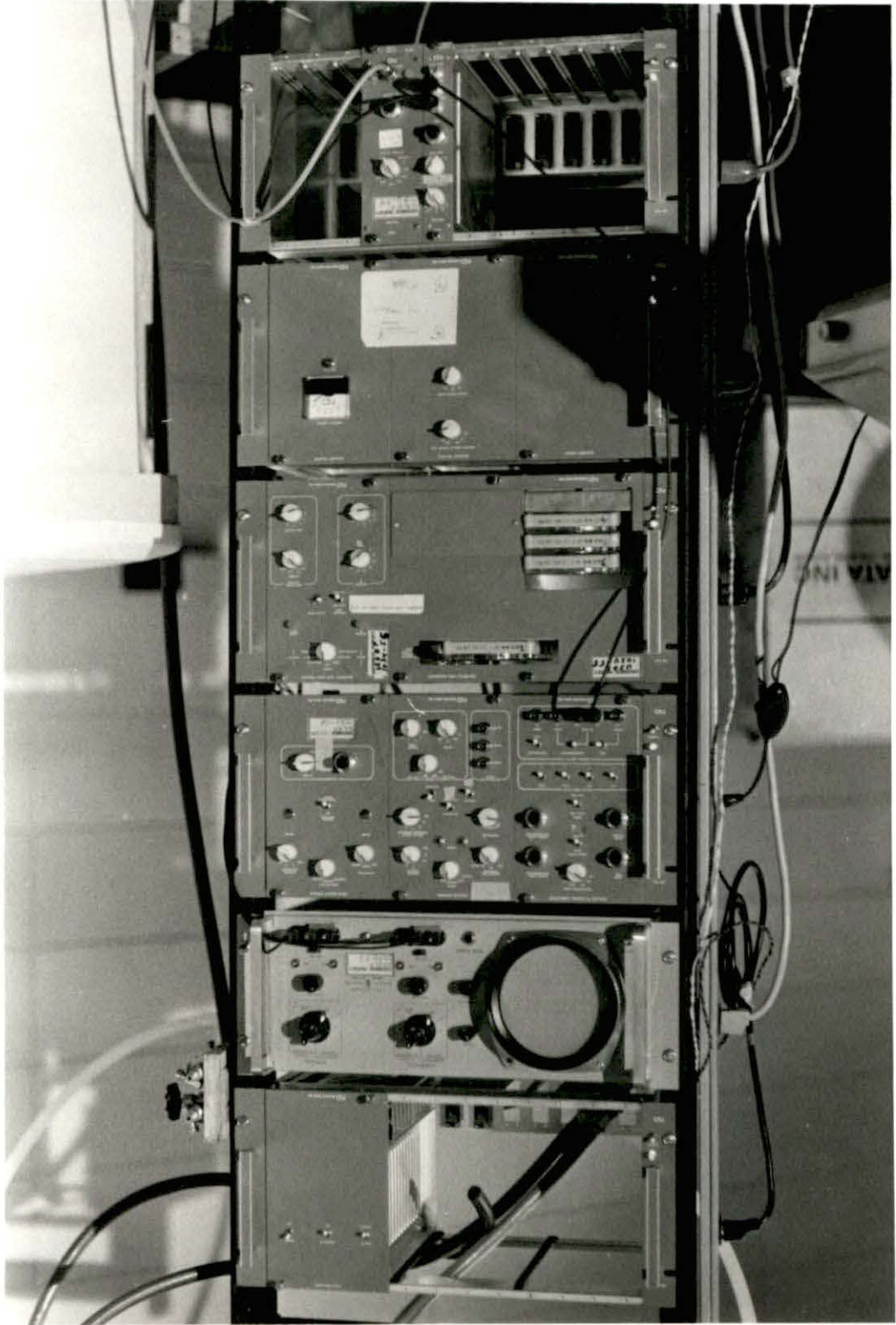
Fig. 9. Heath type cave, Ge(Li) and NaI(Tl) detectors, and sample holder
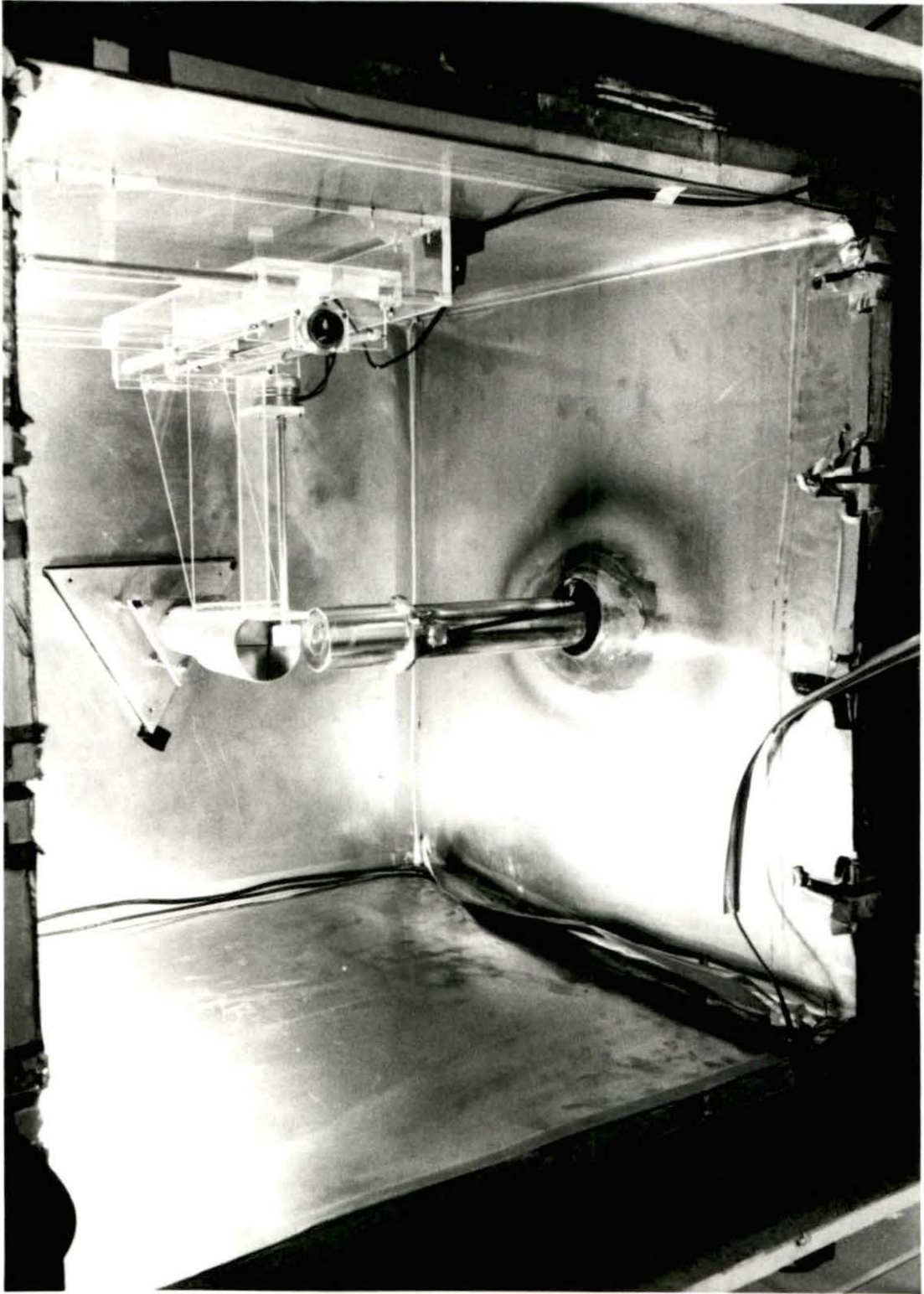
Fig. 10. Close up of rotating sample holder and the Ge(Li) and NaI(Tl) detectors
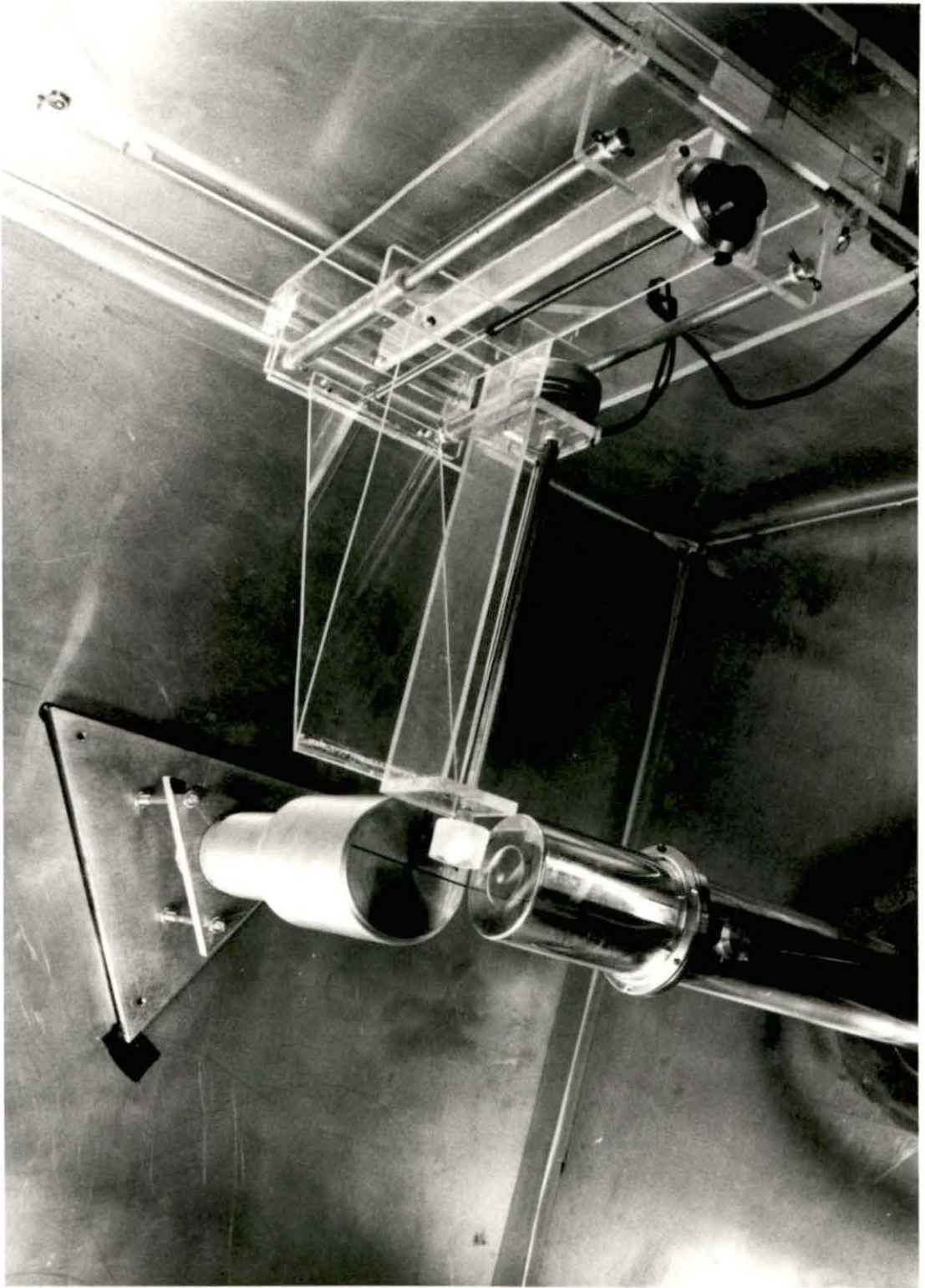
neous background radiation; the cadmium and copper suppress
the lead X rays produced from photoelectric absorption in
the shield; while the large internal dimensions reduce the
backscatter of the gamma rays from the shield walls.

The sample was held at an appropriate counting distance
from either detector by a calibrated adjustable sample hold-
ing device as shown in Fig. 9 and 10. To eliminate differ-
ences in the counting geometry between samples of different
physical configuration, the sample was rotated during count-
ing by a 60 rpm synchronous motor as shown in Fig. 10. Except
for the affect of the spacial variations of detection
efficiency, rotation makes the center of the sample appear
to be at the axis of rotation, regardless of shape.

Two different detectors with their associated preamps
and amplifiers were used: one, a scintillation; the other,
a lithium-drifted germanium device. A complete listing of
all components in this system and their serial numbers may
be found in Appendix D.

Scintillation detector

The scintillation detector is a 3 in. x 3 in. diameter
crystal NaI(Tl) manufactured by Harshaw Chemical Company and
mounted on a RCA 8054 photomultiplier tube. It is shown in
the bottom of Fig. 9. Measurements indicate this detector
has a resolution of approximately 7.3% for the Cs-137, 0.662
Mev photons, and an efficiency versus energy curve as shown

in Fig. 11.

It may be noted that the curve obtained from the
described system is lower than that found by Heath. Heath's
curve is based on a 10 cm source-to-detector distance.
Desiring to make the data in Heath's gamma ray spectrum cata-
log valid for the described system, the source-to-detector
separation was also set at 10 cm. Since the radiation seen
by a detector is inversely proportional to the square of the
source-to-detector separation, the lower curve suggested a
gap between the detector face and the scintillation crystal.
To check this possibility, the crystal was X rayed at the
University Hospital, and the results showed the scintillation
crystal lay 0.45 cm below the crystal face increasing the
nominal 10 cm source-to-detector separation to 10.45 cm.
Calculations indicate that this could cause a 9% lower
efficiency.

Since the NaI detector will detect beta as well as
gamma radiation, it is necessary to prevent the beta parti-
cles from entering the detector. Patterned after Heath's
system, a beryllium metal absorber, 0.65 cm thick, was placed
on the crystal face as a beta absorber.

Lithium-drifted germanium detector

The ORTEC 8200 Ge(Li) detector is a 31.8 mm diameter
coaxially drifted device with an active volume of 21.7 cm^3.
The measured resolution is 4.5 Kev at 1333 Kev while the
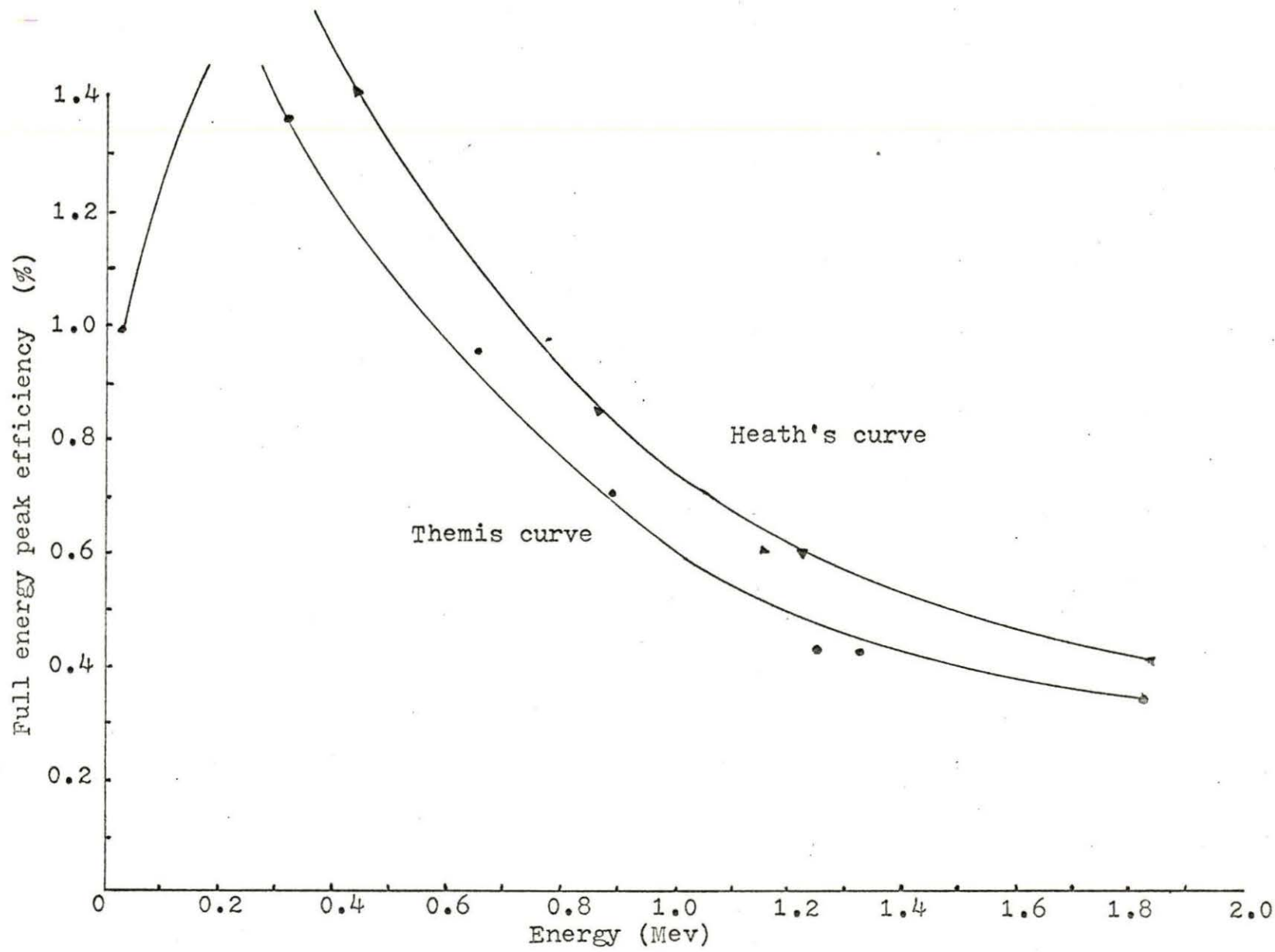
Fig. 11.   Detector efficiency vs energy curve, (NaI) detector

measured "efficiency" ranges from 8% at 360 Kev to 3.5% at
1333 Kev. As is common with Ge(Li) detectors, this effi-
ciency is relative to that of NaI at a given distance and
energy. In this case it is relative to the efficiency of
the NaI detector used as described above. To minimize the
detector-to-preamp cable capacitance in an attempt to achieve
the highest possible resolution, the matching ORTEC 118A
preamp is mounted directly to the cryostat as shown in Fig.
12. The preamp feeds the Nuclear Data mutlichannel analyzer
through an ORTEC 435 amplifier as shown in Fig. 6. To pro-
vide the recommended 3000 v operating bias, a Fluke 405 B
power supply was used. Since the detector must be kept at
liquid nitrogen temperature, it is provided with a 16 liter
dewar which holds approximately a 9-day supply.

The Ge(Li) detector enters the Heath type cave (18)
through the center of the left wall and is positioned in
the center as shown in Fig. 9.

Data handling

The data from the multichannel analyzer is read out
through a Teletype printer and paper punch. Because each
spectrum contains from 256 to 1024 six digit numbers, it
is obvious that analyzing this data by hand would be tedi-
ously time consuming.

A computer program or set or programs meeting the
following criteria was needed:

Fig. 12. A typical Ge(Li) detector, cryostat, and dewar

Note: All dimensions in inches.
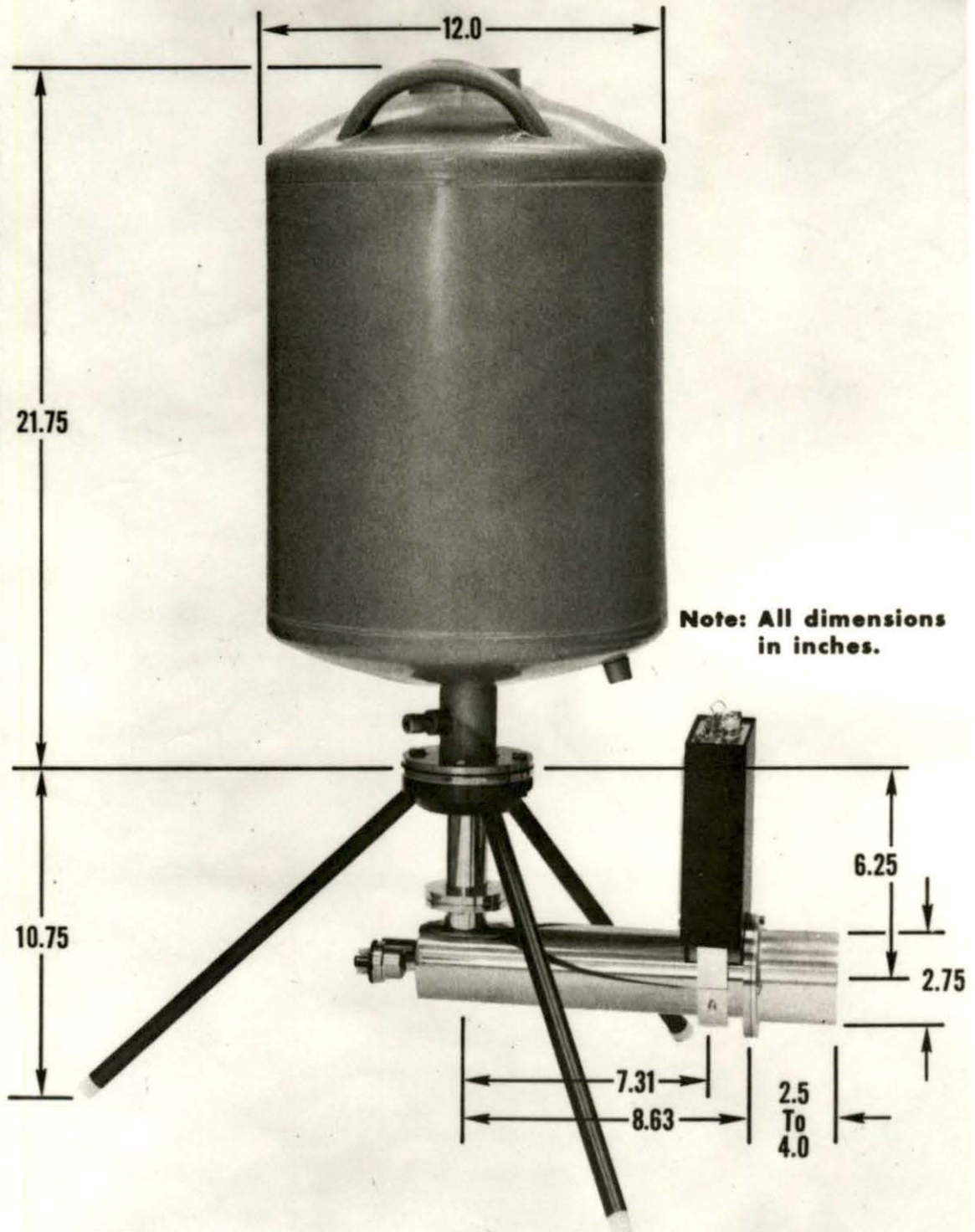
1) Compatibility with the IBM 360/65 system;

2) Capability of analyzing data to find the photo-peaks, their energies, and their areas;

3) Capability of producing plots of spectra;

4) Capability of handling multiple spectra;

5) Adaptability to spectra of different lengths.

After reviewing several existing programs, including Resolf (25) and Alpha (44), and considering the task of writing one, a suitable program entitled ICPEAX-7 (Appendix B) was obtained. ICPEAX-7 requires data in the form of punched cards or a 7-track magnetic tape. In its present form the tape input is limited to 1600 channel data, while the card version will accept any data up to a preset limit. Since our data is in 256, 512, or 1024 sets, the card version was chosen.

To handle the obvious problem of converting the data from punched paper tape to cards, three methods are available:

1) Key punching from the hard copy output;

2) Conversion from punched paper tape to punched card using the IBM-47 convertor at the I.S.U. Synchrotron facility;

3) Conversion from punched paper tape to magnetic tape using the facilities at the I.S.U. Cyclone Computer Center. The magnetic tape can be used to feed the data to the IBM 360/65 which will, with the program "PRESTO" (Appendix B), punch the data on cards in a suitable format.

CHAPTER IV. QUALITATIVE ANALYSIS

The qualitative analysis was divided into several parts; the first of which was a study of the feasibility of using instrumental neutron activation to analyse a magnesium oxide crystal. Included were a study of the nuclear and physical properties of the magnesium oxide, a safety analysis both with respect to the reactor and the experimenter, and a study of the nuclear properties of the impurities expected. Preliminary irradiations pointed out problems with sample contamination and fast reactions. Furthermore, these irradiations provided an opportunity to check out the detector-analyser system and develop experimental techniques. The technique used in the qualitative analysis was to begin with a short irradiation at a low flux, counting the sample immediately after irradiation, and continuing the count until all activity had subsided. This procedure was repeated at higher and higher neutron flux doses until a maximum irradiation of approximately 4×10^{17} nvt was used. At the higher irradiation levels, counting was delayed for several days to allow short lived activities to decay.

Properties of Magnesium Oxide

Periclase, which in Greek means "beyond breaking", is the minerological name for magnesium oxide. It is a high

temperature refractory material characterized by a strong
ionic bond between the divalent magnesium and oxygen atoms.
Magnesium oxide has a rock salt structure and its deviation
from stochiometry is so small that it has not been measured.
Some of the physical and nuclear properties of magnesium
oxide are listed in Tables 2 and 3.

Single crystals of magnesium oxide can accommodate
small amounts of impurities in either substitutional or
interstitial positions in the crystal lattice. Furthermore,
many transition metal ions have radii near enough to magne-
sium's to be easily accommodated. These impurities may have
a strong influence on the physical properties of a single
crystal such as ionic conductivity, optical absorption,
dielectric loss, and creep properties.

It is apparent from Tables 2 and 3 that magnesium oxide
is a favorable matrix for activation analysis because the
oxygen is virtually inert to thermal neutrons, and the mag-
nesium produces only short-lived isotopes.

Safety Considerations

Magnesium oxide is physically stable, nonflammable and
nontoxic so that the only hazard stems from the neutron
induced radioactivity. To protect the reactor and experi-
menter from hazardous radioactive contamination, the samples
were encapsulated in snap-top polyethylene vials which
during irradiation were sealed in polyethylene envelopes.

Table 2.   Physical properties of MgO

Element	Form	Molecular weight	Density gm/cm^3	Melting point	Boiling point	Solvent
Magnesium oxide (MgO)	crystal	40.31	3.58	2800°C	3600°C	Boiling phosphoric acid

Table 3.   Nuclear properties of MgO

Element	Abundance (%)	Reaction	Product nuclide	Cross section (barns)	Half-life of product	γ ray (Mev)	
^{26}Mg	11.29	n, γ	^{27}Mg	0.027	9.46 min	0.84 (70%)	1.013 (30%)
^{24}Mg	78.60	n, p	^{24}Na	0.19	14.97	1.37 (100%)	2.75 (100%)

The possibility that radiation heating in the magnesium oxide crystal might cause the capsule to melt was considered. Because magnesium has a small nuclear cross section this possibility was judged remote while experiments at increasing flux doses verified that no heating problem existed. The limiting factor appeared to be radiation damage in the polyethylene at integrated neutron fluxes greater than 4×10^{17} nvt.[1] For this reason, the irradiations in this work were restricted to less than 4×10^{17} nvt.

In addition to the above precautions, all samples were routinely monitored by Health Physics after irradiation and stored in a lead chamber when not in use. Irradiated samples were handled with either rubber gloves or forceps to prevent contact with the experimentors skin and all radioactive samples or their containers were plainly marked with the appropriate warning.

Development of Technique

Qualitative activation analysis involves a binary decision. Either an element is or is not detected. In practice, the analysis may be confused by a number of factors including several nuclides emitting the same or approximately the same energy gamma rays, contamination of the sample prior to

---

[1]Link, Bruce W., 225 Reactor, Ames Lab, Ames, Iowa. Sample preparation. Private communication. 1969.

irradiation, or nuclides present in trace amounts approaching the sensitivity of the analysis and competing fast reactions. In addition, it is very difficult to analyse for nuclides whose activity has a half-life of the same order of magnitude as that of matrix elements.

Removal of surface contamination

Since surface impurity concentrations may confuse the analysis, it was necessary to perfect cleaning techniques for both the samples and the encapsulation container. Initially, acetone had been used to wash or rinse these items, but experiments showed that acetone was not able to consistently remove the NaCl contamination from finger-prints. This could be explained by acetone's inability to remove grease effectively.

The problem was divided into two parts: first, to find a suitable cleaning agent for the MgO and second, to find one for the polyethylene capsules. After searching for a precedent, it was found that phosphoric acid had been used in the past on $MgAl_2O_4$ Spinel crystals.[5]

One effective way to clean the crystals is to remove the surface containing the contamination. This etching may be done either before or after the irradiation. If done

after, the contamination introduced by the etching agent is
of no concern since it will not be activated and hence will
not be detected. The primary concern is that all surface
contaminants be removed exposing only virgin crystal. This
process has the obvious shortcoming that radiochemistry is
involved requiring a hot lab. Since no hot lab was con-
veniently available, this technique was abandoned in favor
of etching before irradiation.

Again it is of primary importance that all of the sur-
face contaminants be removed; and, in addition, that the
etching agent, which itself may contaminate the crystal, be
radioactively inert so that it does not affect the analysis.

Experiments measuring the weight loss of an MgO crystal
boiled in phosphoric acid confirmed that it is etched by the
acid. Furthermore, the phosphorous contamination which may
take place during the etching should present no problem
because the $^{31}_{15}P$ isotope which comprises 100% of naturally
occurring phosphorous does not emit ν-radiation upon activa-
tion and hence will not be detected. Special precautions,
discussed later in this section, were taken to insure that
samples, once etched, would not be contaminated before or
during the irradiation.

The polyethylene capsules, it was found, could be effec-
tively cleaned in approximately 7M nitric acid. Other less
satisfactory techniques included triply rinsing the capsules

in acetone, ether, alcohol, and trichloroethylene. The technique adopted consists of stirring the capsules in nitric acid for 5 min, removing them with a glass rod, and stirring them in distilled water for 5 more min. They are then heated in an oven at 80° C for several hours until dry. An experimental activation confirmed that this cleaning technique is effective in removing contamination.

Preparation of the MgO sample

In searching for a suitable physical form in which to analyze the crystal by activation, the following factors were considered:

1) Self-shielding,

2) Possibility of contamination of the sample,

3) Ease of cleaning surface contaminants from the sample,

4) Ease of preparing the sample,

5) Ability to analyze a sample in the form used by other research groups,

6) Homogeny of the sample.

A preparation technique used by Hee Myong Lee (30) was to grind the MgO crystal in a ball mill and treat it as a powder. If a large enough sample is ground up, this method insures homogeny. To check the feasibility of using this method, a sample of MgO crystal was ground in a Pica Blender Mixer. The mill used has two different types of canisters:

one is made of tungsten; and the other, of stainless steel.
Grinding a pre-etched sample in each, the following results
were noted:

1) The samples increased in volume as they were ground.

2) They changed from clear to a dull, gray-white color.

3) An activation analysis showed that both samples
   picked up severe contamination from their respective
   canisters.

The contamination from the steel canister could not be
tolerated because Fe is a trace element expected to be
present in MgO. While tungsten is not expected, it is
possible that there are trace amounts of other elements
being introduced with the tungsten. It was decided to look
for a different method of sample preparation which would
avoid this contamination.

The MgO samples to be analyzed from the Themis (5)
creep-test lab were in the form of rectangular solids
approximately 0.38 x 0.38 x 0.76 cm with a weight of 0.3 gm.
These specimens were all cut to approximately the same size
and shape, and the exact dimensions of each were measured
with a micrometer. Using these crystals in this configura-
tion simplified sample preparation, permitted a nearly
nondestructive analysis and analyzed the actual crystal
being tested in the creep-test lab.

A self-shielding calculation was carried out to deter-

mine the magnitude of the self-shielding factor associated
with a MgO sample of this size and shape (18, 23, 38). Since
the MgO crystal of interest is 99.99% pure, the impurities
do not contribute to the self-shielding; and the MgO matrix,
due to its low cross section, exhibits very little self-
shielding. Calculations in Chapter VI show that a solid
crystal of MgO, 0.38 x 0.38 x 0.74 cm would have a self-
shielding factor of approximately 1.0 (i.e., no self-
shielding).

The actual technique used to prepare MgO samples con-
sisted of obtaining a precut MgO crystal specimen from the
creep testing lab and measuring its dimensions with a
micrometer. The crystal was then placed in a test tube
containing phosphoric acid and boiled for 2 min over an open
flame. After cooling, the acid was poured off, and the test
tube containing the crystal was flushed thoroughly with
distilled water followed by acetone. The crystal was then
dumped onto a fresh piece of filter paper to be dried under
an infrared lamp. A clean forceps, freshly rinsed with
acetone and heat dried, was used to transfer the cleaned
and dried crystal to a fresh slip of weighing paper. After
weighing the sample with the Gram-atic Balance (serial 1-910),
clean forceps were used to place it inside a polyethylene
capsule. This capsule then was sealed inside a polyethylene
envelope and put in a capsule with a slightly larger diameter

to maintain alignment with two similar samples as shown in
Fig. 13. The larger capsule is then packed in a rabbit
for irradiation.

In an attempt to make a qualitative impurity determina-
tion, preliminary irradiations of the MgO crystal were
carried out in the rabbit facility of the UTR-10 reactor.
Encapsulated MgO samples were irradiated at a power of 10 kw
(7×10^6 n/cm^{2}sec) for periods of 15 min to 4 hr. Counting
was done with the NaI detector starting approximately 3 min
after the irradiation. Three min is the minimum time needed
to monitor the sample and transport it to the detector.
Counting continued for several days until all activity had
subsided. Before counting, the polyethylene capsules were
opened and vented to permit the small but detectable amount
of argon to escape. Argon, as found in the atmosphere, under-
goes a ^{40}Ar(n,γ)^{41}Ar reaction with thermal neutrons producing
1.293 Mev gamma activity with a half-life of 1.83 hr. The
cross section for the reaction is 0.61 b. It is conceivable
that this full-energy peak could mask or interfere with the
analysis for other elements should they emit photons with
approximately the same energies.

These UTR-10 irradiations revealed not only the magnesium
of the matrix, but also manganese and sodium. These results
were disappointing because Lee (30) had reported, in addition
to manganese, traces of longer half-life elements including

Scale: actual size

MgO
crystal

polyethylene
packing

2/5 dram
polyethylene
capsule
1.2 cm O.D.

polyethylene
envelope

envelope
heat sealed

51

standard
1

MgO
sample

standard
2

large polyethylene capsule
1.6 cm I.D.
7.6 cm length

ALRR rabbit
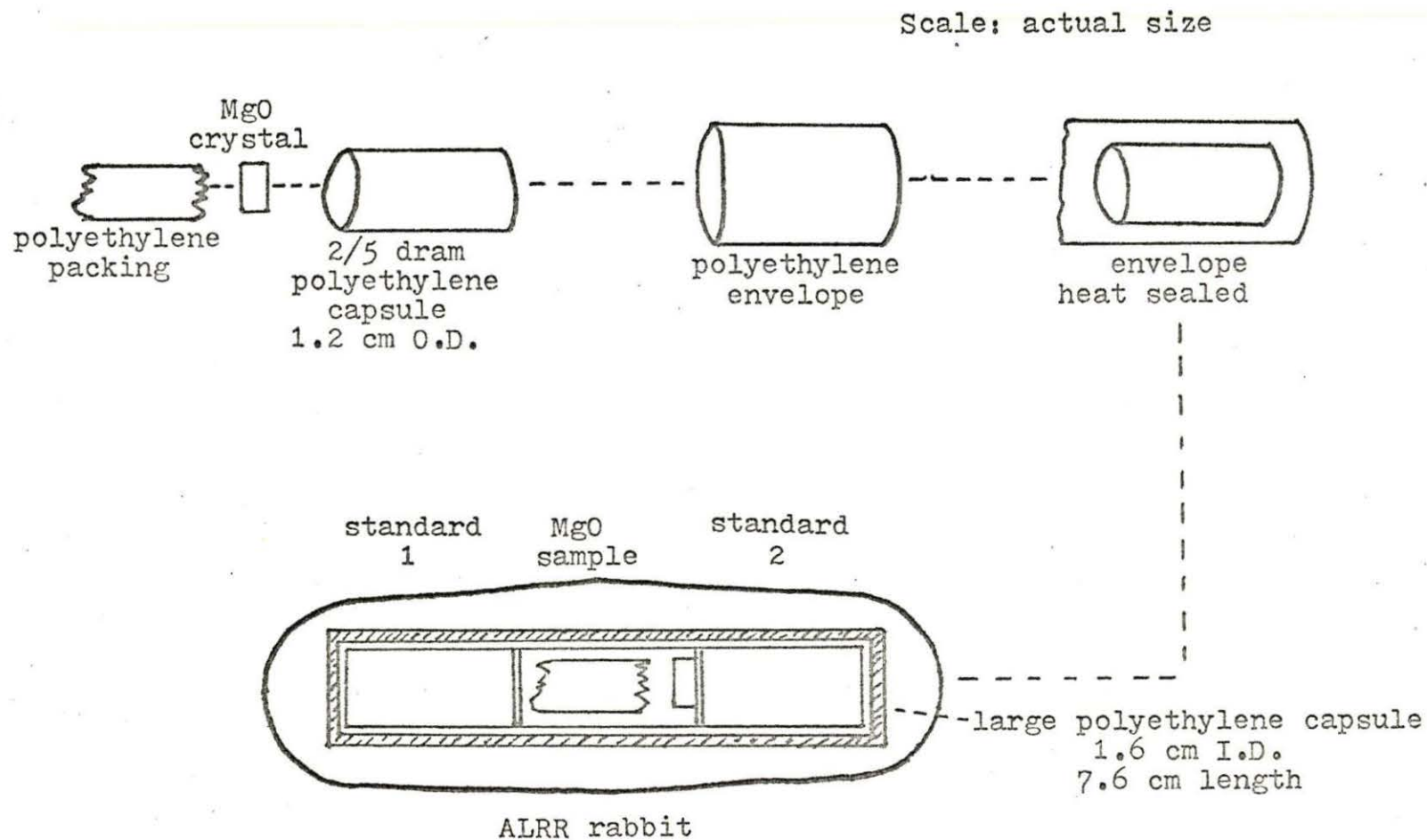
Fig. 13.   Sample encapsulation technique

iron, chromium, and scandium, in a similar crystal. An emission spectrometric analysis, as shown in Fig. 14, indicated still other possible impurities. It was concluded that either the other impurities were not present or, because of their long half-lives and small cross sections, a higher integrated flux was needed to activate them as illustrated by Tables 4, 5, and 6. Furthermore, there was some doubt as to the origin of the sodium detected in these UTR-10 irradiations. The sodium could be present in the crystal matrix, be a surface contaminant introduced by handling, or be the result of the reaction, $^{24}Mg(n, p)^{24}Na$ listed in Table 3.

Analysis for Long Half-Life Impurities

Because the presence of sodium would not interfere with the analysis of the expected long half-life elements as shown in Tables 5 and 6, and because the analysis of these elements would require decay periods of 1 to 2 weeks; the sodium problem was temporarily put aside. In an attempt to identify the long half-life elements, a magnesium oxide sample was prepared as before and irradiated for 1 hr at 5 mw in position R-3 of the ALRR facility (flux = 3.4×10^{13} n/cm^2sec, cadmium ratio approximately 20). After waiting 14 days for the magnesium, manganese, and sodium activities to subside, the magnesium oxide crystal was removed from its irradiation container and counted for 3 hrs on the Ge(Li)

Fig. 14. Qualitative emission spectroscopic analysis of
magnesium oxide crystal

AMES LABORATORY

ANALYTICAL SERVICES GROUP II
EMISSION SPECTROSCOPY

ANALYTICAL REPORT FORM
(request must be submitted in duplicate)

Date Submitted __3 · /21/ 69__

Date Reported __4 /2 /69__

Description of Sample __M$_g$O Crystals (G.E.)__

To Be Analyzed For __COMPLETE QUAL__

Type of Analysis: Qual. __✓__, Semiquant. _____, Quant. _____

Requested By __MF BERARD__

Room __22__   Bldg. __MET__

Tel. __4-1976__ Act. No. _____

Group Leader's Approval _____

NOTE: Samples not picked up within 10 days of report date will be discarded.

Sample No.														

Values are in ppm _____ : % _____ by weight in metal _____ oxide _____

Remarks

Symbol	Meaning	
(A)	Within 50% of amt. reported	
(B)	Within 20% of amt. reported	
(C)	Within 10% of amt. reported	
(D)	Within 5% of amt. reported	
(E)	Within 2-3% of amt. reported	
VS	Very Strong	Major
S	Strong	Constituent
M	Moderate	Minor
W	Weak	Constituent
VW	Very Weak	Trace
T	Trace	Impurity
FT	Faint Trace	
d	ele detected	
—	ele not detected	
>	greater than	
<	less than	
X	interference	
	ele not investigated	

Analysis by: __De Kalb__

Plate number: __52680, 5__

4 3 68

ELE			ELE			ELE			ELE			ELE		
Ag	—		Dy			Lu			Rb	—		Tl	—	
Al	—		Er			Mg	VS		Re	—		Tm		
As	—		Eu			Mn	T		Rh	—		U	—	
Au	—		Fe	TV W		Mo	FTX		Ru	—		V	—	
B	—		Ga	—		Na	—		Sb	—		W	—	
Ba	FTX		Gd			Nb	—		Sc	—		Y	—	
Be	—		Ge	—		Nd			Si	FTX		Yb		
Bi	—		Hf	—		Ni	FTX		Sm			Zn	—	
Ca	VW		Hg	—		Os	—		Sn	—		Zr	—	
Cd	—		Ho			P	—		Sr	—				
Ce			In	—		Pb	—		Ta	—				
Co	—		Ir	—		Pd	—		Tb					
Cr	T		K	—		Pr			Te	—				
Cs	TX		La	—		Pt	—		Th	—				
Cu	T		Li	—		Ra			Ti	T				

Table 4. Relevant nuclear properties of short half-life impurities[a]

Parent nuclide	Isotope	Abundance (%)	Reaction	Product
Silicon	^{28}Si	92.27	(n,p)[c]	^{28}Al
	^{29}Si	4.68	(n,p)[c]	^{29}Al
	^{30}Si	3.05	(n,α)[c]	^{27}Mg
Phosphorous	^{31}P	100	(n,α)[c]	^{28}Al
Calcium	^{48}Ca	0.185	(n,γ)	^{49}Ca
Titanium	^{50}Ti	5.25	(n,γ)	^{51}Ti
Chromium	^{54}Cr	2.4	(n,γ)	^{55}Cr
Cobalt	^{59}Co	100	(n,γ)	^{60m}Co
Copper	^{63}Cu	69.1	$(n,2n)$[c]	^{62}Cu

[a] 1 min to 1 hr, Lederer, Hollander and Perlman (28).

[b] 1 hr irradiation at a thermal flux of 1×10^{12} $n/cm^2 sec$, Moses (34).

[c] Fast activation data, Moses (34).

Cross section (barns)	Half-life of product (min)	γ ray (Mev)			Specific activity[b] (dpm/ug)
0.22	2.30	1.73 (100%)			263
0.10	6.56	1.28, (85%)	2.93 (15%)		6
0.08	9.45	0.84, (100%)	1.02 (30%)		3
0.150	2.3	1.78 (100%)			175
1.1	8.8	3.10, (89%)	4.10, (10%)	4.68 (3%)	1.8×10^3
0.14	5.79	0.32, (95%)	0.605, (1.5%)	0.928 (5%)	5.6×10^3
0.38	3.6	none			none
18	10.5	0.059, (2.1%)	1.33 (0.25%)		9.8×10^6
0.500	9.8	0.66, (2%)	0.85 (1%)		197
		1.18, (1%)	1.35 (1%)		

Table 4.   (Continued)

Parent nuclide	Isotope	Abundance (%)	Reaction	Product
Copper	^{65}Cu	30.9	(n,γ)	^{66}Cu
Bromine	^{79}Br	50.52		^{80}Br
Molybdenum	^{92}Mo	15.86	$(n,2n)^c$	^{91}Mo
Antimony	^{121}Sb	57.25	(n,γ)	^{122m}Sb
Barium	^{136}Ba	71.66	(n,γ)	^{137}Ba

Cross section (barns)	Half-life of product (min)	γ ray (Mev)		Specific activity[b] (dpm/ug)
2.3	5.1	1.039 (9%)		3.1×10^5
8.5	17.7	0.511, (5%)	0.618 (7%)	
0.190	15.5	none		10
0.06	4.2	0.061, (50%)	0.075 (17%)	3.2×10^4
0.01	2.6	0.662 (89%)		1.0×10^4

Table 5. Relevant nuclear properties of intermediate half-life impurities[a]

Parent nuclide	Isotope	Abundance (%)	Reaction	Product
Silicon	^{30}Si	3.12	(n, γ)	^{31}Si
Phosphorous	^{31}P	100	(n, p)[c]	^{31}Si
Manganese	^{55}Mn	100	(n, γ)	^{56}Mn
Copper	^{63}Cu	69.1	(n, γ)	^{64}Cu
	^{65}Cu	30.9	(n, 2n)[c]	^{64}Cu
Nickel	^{64}Ni	1.16	(n, γ)	^{65}Ni
Bromine	^{81}Br	49.48	(n, α)[c]	^{78}As
			(n, 2n)[c]	^{80}Br
Molybdenum	^{97}Mo	9.45	(n, p)[c]	^{97}Nb
Cesium	^{133}Cs	100	(n, γ)	^{134}Cs
Barium	^{138}Ba	71.66	(n, γ)	^{139}Ba

[a] 1 hr to 1 day, Lederer, Hollander and Perlman (28).

[b] 1 hr irradiation at a thermal flux of 1 x 10^{12} n/cm^2 sec, Moses (34).

[c] Fast activation data, Moses (34).

Cross section (barns)	Half-life of product (hr)	γ ray (Mev)			Specific activity[b] (dpm/ug)
0.11	2.62	1.26 (0.07%)			8.8×10^2
0.077	2.62	1.26 (0.07%)			21
13.3	2.58	0.847, (99%)	1.81, (29%)	2.11 (15%)	2.2×10^6
4.5	12.9		1.34, (0.5%)	0.51 (38%)	8.1×10^4
1.0	12.9		1.34, (0.5%)	0.51 (38%)	10
1.5	2.56	0.368, (4.5%)	1.115, (16%)	1.481 (25%)	2.8×10^3
0.10	1.5	0.62, (42%)	0.70, (11%)	1.31 (10%)	8
0.800	4.58		0.037, (100%)	0.099 (100%)	27
0.110	1.2		0.69, (99%)	1.02 (1%)	2
2.6	2.9		0.128 (14%)		1.0×10^3
0.4	1.42		0.166, (23%)	1.43 (0.4%)	3.7×10^4

Table 6. Relevant nuclear properties of long half-life impurities[a]

Parent nuclide	Isotope	Abundance (%)	Reaction	Product
Phosphorous	^{31}P	100	(n, γ)	^{32}P
Calcium	^{44}Ca	2.06	(n, γ)	^{45}Ca
Scandium	^{45}Sc	100	(n, γ)	^{46}Sc
Chromium	^{50}Cr	4.3	(n, γ)	^{51}Cr
Iron	^{56}Fe	91.66	(n, p)[c]	^{56}Mn
	^{58}Fe	0.31	(n, γ)	^{59}Fe
Cobalt	^{59}Co	100	(n, γ)	^{60}Co
Bromine	^{81}Br	49.48	(n, γ)	^{82}Br
Molybdenum	^{98}Mo	23.75	(n, γ)	^{99}Mo

[a] 1 day or greater, Lederer, Hollander and Perlman (28).

[b] 1 hr irradiation at a thermal flux of 1×10^{12} n/cm^2 sec, Moses (34).

[c] Fast activation data, Moses (34).

Cross section (barns)	Half-life of product	γ ray (Mev)			Specific activity[b] (dpm/ug)
0.191	14.6 days	none			4.8×10^2
0.63	160 days	none			2.1
12	84 days	0.89, (100%)	1.12 (100%)		4.4×10^3
17.5	27.8 days	0.32 (10%)			4.0×10^2
0.110	2.58 hr	0.84, (99%)	1.81, (29%)	2.11 (15%)	2.2×10^6
1.1	45.1 days	1.095, (56%)	1.292 (44%)		1.3
20	5.3 yr	1.17, (100%)	1.33 (100%)		3.2×10^2
3.0	35.5 hr	0.554, (66%)	0.619, (41%)	0.698 (27%)	1.6×10^4
		0.777, (83%)	0.828, (25%)	1.317 (26%)	
		1.475 (17%)			
0.51	2.75 days	0.181, (67%)	0.74, (12%)	0.78 (4%)	4.4×10^2

Table 6.   (Continued)

Parent nuclide	Isotope	Abundance (%)	Reaction	Product
Antimony	^{121}Sb	57.25	(n, γ)	^{122}Sb
	^{123}Sb	42.75	(n, γ)	^{124}Sb
Barium	^{130}Ba	0.101	(n, γ)	^{131}Ba
	^{132}Ba	0.097	(n, γ)	^{133m}Ba
	^{132}Ba	0.097	(n, γ)	^{133}Ba
	^{134}Ba	2.42	(n, γ)	^{135m}Ba
Cesium	^{133}Cs	100	(n, γ)	^{134}Cs

Cross section (barns)	Half-life of product	γ ray (Mev)				Specific activity[b] (dpm/ug)
6.0	2.8 days	0.564, (66%)	0.686 (3%)			1.3×10^4
3.3	60 days	0.603, (97%)	0.72, (14%)	1.69 (50%)		1.5×10^2
8.8	11 days	0.12, (28%)	0.216, (19%)	0.373, (13%)	0.496 (48%)	7.3
0.2	1.63 days		0.276 (100%)			3.5×10^1
7	7.2 years	0.082, (25%)	0.276, (7%)	0.302, (14%)	0.356 (69%)	1
0.16	1.21 days		0.268 (16%)			3.4×10^2
28	2 years	0.57, (23%)	0.605, (98%)	0.798 (99%)		3.6×10^2

detector RIDL 1600 channel analyzer system available at the
ALRR facility. The resulting spectrum shown in Fig. 15
indicates the following:

^{51}Cr at 0.32 Mev

^{122}Sb at 0.564 and 0.686 Mev

^{124}Sb at 0.603 and 1.69 Mev

^{46}Sc at 0.89 and 1.12 Mev

^{59}Fe at 1.095 and 1.292 Mev

^{60}Co at 1.17 and 1.33 Mev

The relevant nuclear properties of these and other possible
long half-life impurities are given in Table 6. Of the
activities listed above, all but antimony were expected and
gave positive identification when compared to Heath's catalog
of spectra and when the characteristic half-lives were con-
sidered. Two verification activations, Exp 8-7-69 and Exp
8-26-69, confirmed the above results. These latter two
experiments also showed bromine in the spectra taken within
several days of the irradiation. An analysis of an empty
capsule, a capsule filled with water evaporated to dryness,
and a capsule containing a magnesium oxide sample showed an
equal level of bromine in each. Therefore, the bromine was
judged to be a constituent of only the capsule.

To check the possibility that antimony was introduced by
the phosphoric acid used to etch the crystal, a 10 λ sample
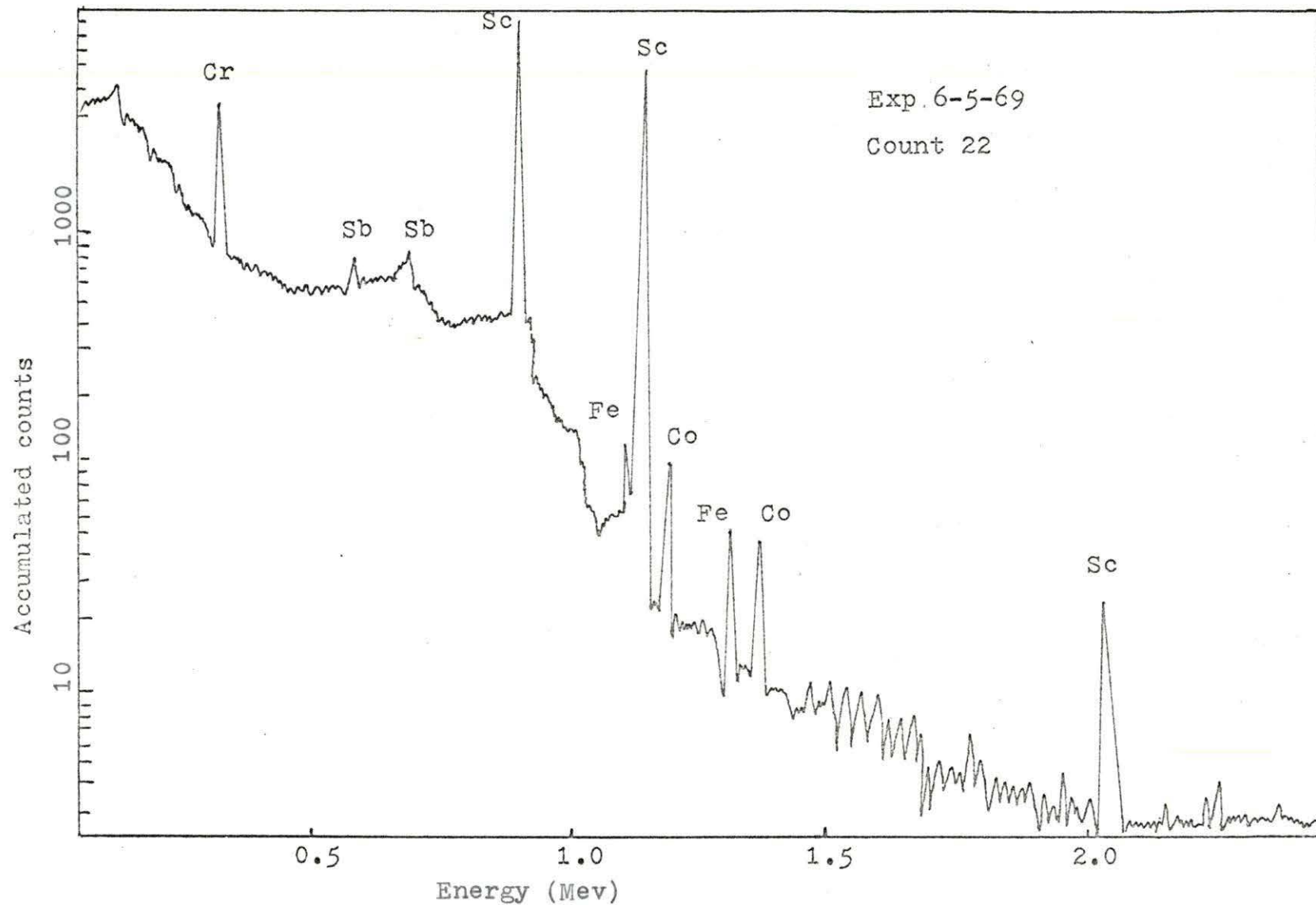was activated along with the crystal in Exp 8-26-69. The

Fig. 15. Spectrum showing long half-life activities in an MgO crystal

analysis of the acid showed positive evidence of antimony as shown in Fig. 16. As a further check, the magnesium oxide crystal analyzed in Exp 8-26-69 was given a much more thorough flush with distilled water after the pre-irradiation acid etch than had been the practice. The full-energy peak area ratio of antimony to the scandium for this experiment is 0.14 as compared to 0.16 for previous experiments. This leads to the conclusion that the antimony is a contaminant left by the phosphoric acid. Further work in this area is suggested.

Analysis for Intermediate Half-Life Impurities

Before a sensitive qualitative analysis for the intermediate half-life impurities shown in Table 5 could be made, the high sodium activity had to be removed. As noted before, sodium could be present as a constituent of the crystal matrix, a surface contaminant introduced by handling, or a result of the fast reaction, $^{24}Mg(n,p)^{24}Na$, listed in Table 3.

Since sodium's nuclear properties make it easily activated (Na-24, cross section = 0.51 b, isotopic abundance = 100, half-life = 14.97 hr), it can be detected readily with a short irradiation. Past experience has shown that even the sodium chloride in fingerprints can be detected with a 10 kw, 15 min irradiation in the rabbit facility of the UTR-10. A 15 min irradiation of the magnesium oxide crystal in this facility showed only mild sodium activity and no chlo-
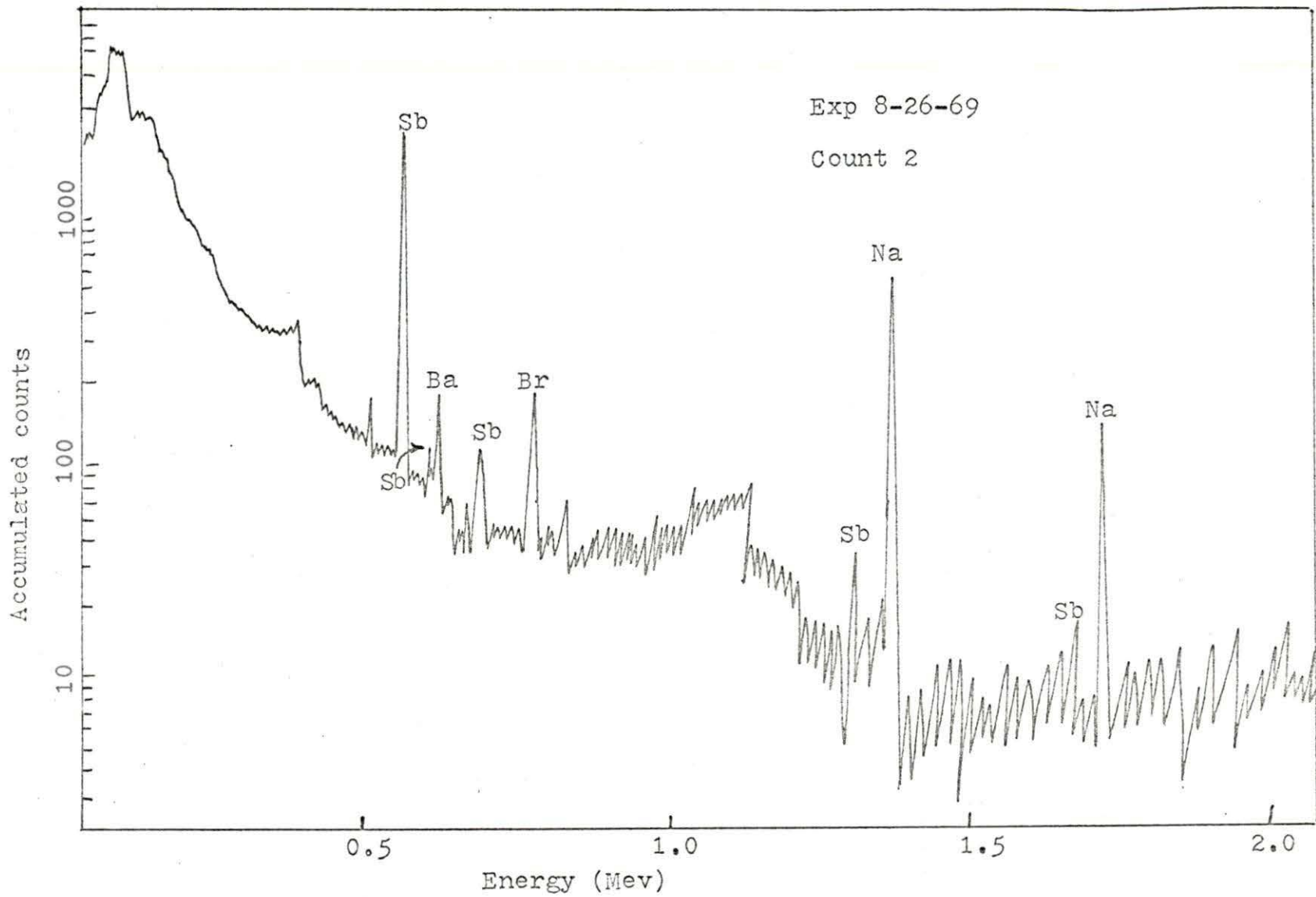
Fig. 16. Spectrum of phosphoric acid

rine activity. The lack of chlorine activity indicated that the sodium was not the result of sodium chloride surface contamination from fingerprints. The low sodium activity re-enforced the idea that the sodium was not present in the sample but was a result of the Mg(n,p)Na reaction. Since the cadmium ratio of the rabbit facility in the UTR-10 is only approximately 6, this fast neutron reaction is quite likely.

To remove all doubt, the magnesium oxide crystal was irradiated for 1 hr at 5 mw in location TV1 of the ALRR facility (flux = 6 x 10^{10} n/cm^2sec, cadmium ratio 1000). This irradiation, as shown in Fig. 17, resulted in no measurable sodium activity indicating the sodium activity found in the previous samples was a result of the Mg(n,p)Na reaction. (Since an (n,p) reaction with iron produces manganese-56 i.e., ^{56}Fe(n,p)^{56}Mn as shown in Table 6, and since it is desired to determine manganese in the presence of iron; this experiment also indicated that manganese determinations would require an irradiation in a high cadmium ratio location. This is especially true since the amount of iron expected is an order of magnitude larger than the manganese, and the iron-56 isotope is about 300 times more abundant than the iron-58 isotope. This makes the ^{56}Fe(n,p)^{56}Mn reaction about as sensitive as the ^{58}Fe(n,γ)^{56}Fe reaction.) (See Table 6.)

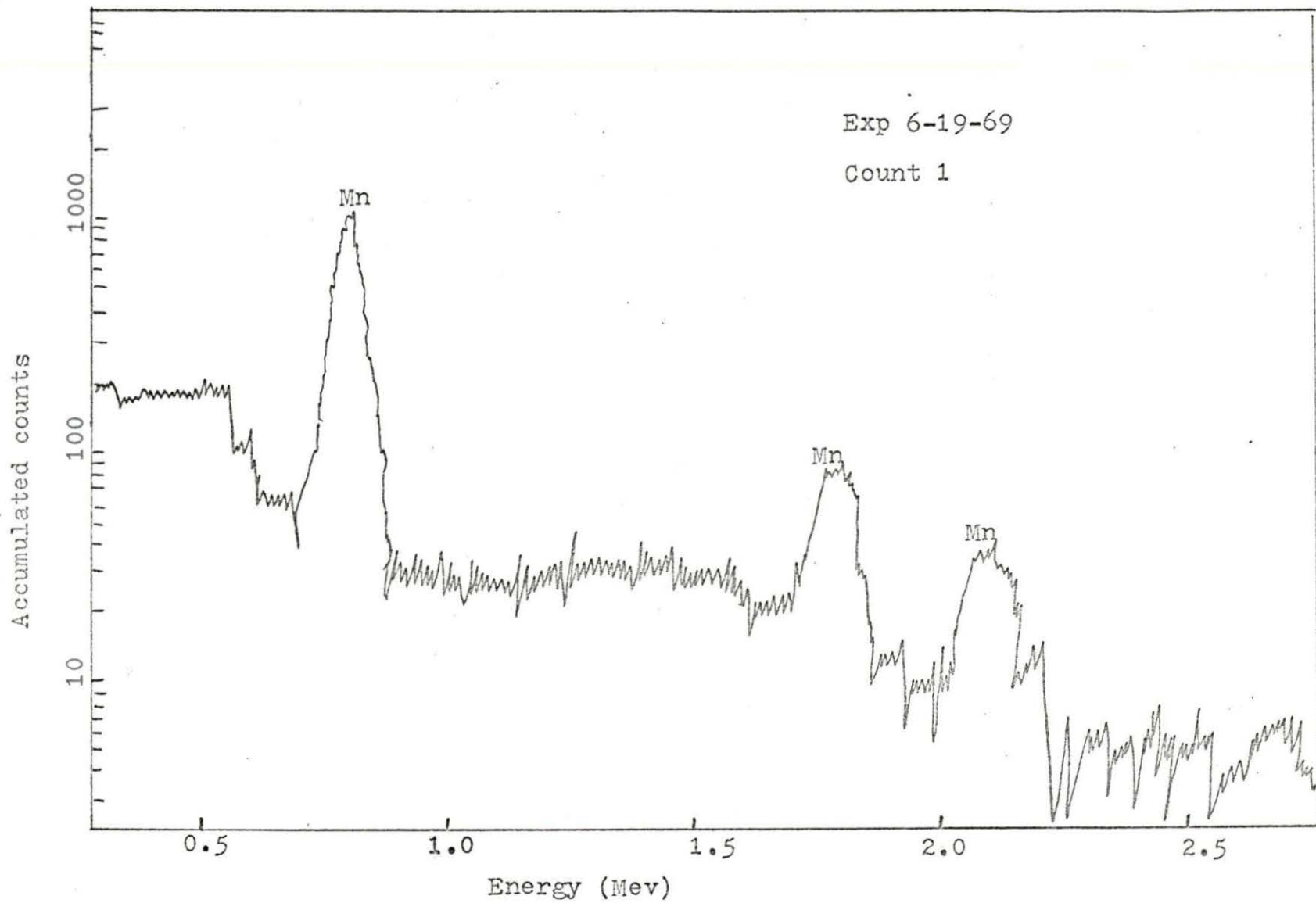The lack of sodium activity, which had been very high

Fig. 17.   Spectrum showing no Na^{24} activity in a thermal irradiation of MgO

in the past, produced a much cleaner spectrum. Counting 2 hrs after irradiation, with the NaI detector produced the spectrum shown in Fig. 17. The peaks are the 2.58 hr manganese activity at 0.847, 1.81, and 2.11 Mev. Twelve hrs later these had decayed, and only insignificant background was seen. This manganese identification was confirmed by the analysis of two similar irradiations in TVl of the ALRR facility.

The activities from these later irradiations which were counted on the Ge(Li) detector indicated the possible presence of copper. Copper is hard to identify because, as shown in Table 5, the only sensitive reaction is $^{63}Cu(n,\gamma)^{64}Cu$ which produces annihilation radiation at 0.51 Mev and a weak peak at 1.34 Mev which is often lost in the background. The suggestion that copper is present is based on the 0.51 Mev peak and a half-life determination. The other nuclides producing activities of 0.51 Mev either have vastly different half-lives or multiple peak spectra. (See Fig. 18)

Analysis for Short Half-Life Impurities

While the 9.5 min half-life activity of the manganese-27 matrix facilitates the detection of elements with half-lives greater than one hr, it makes the detection of shorter lived elements difficult or impossible. In theory it is possible to detect short lived elements in the presence of long lived ones by irradiating for a short duration with respect to the
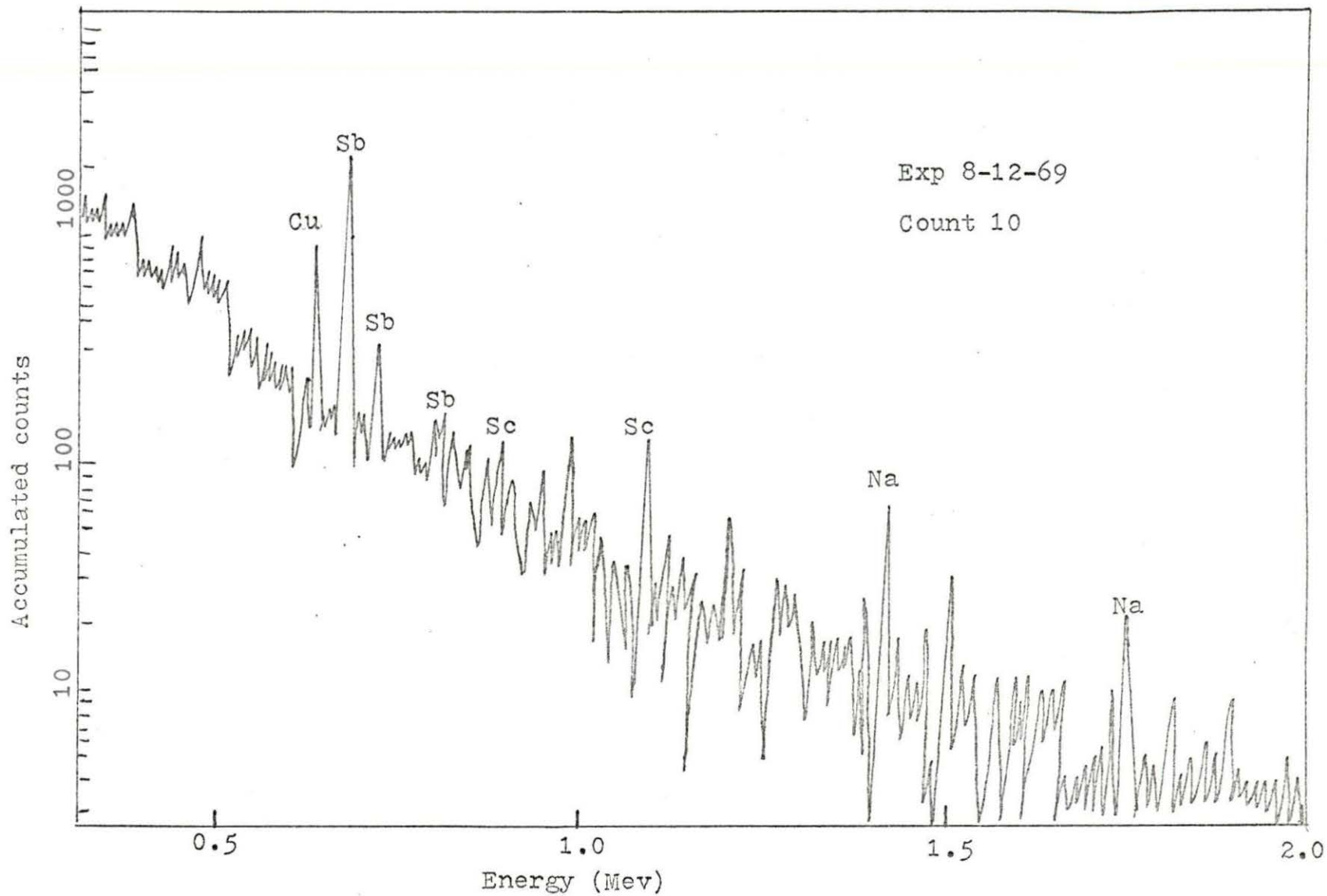
Fig. 18.   Spectrum of MgO crystal showing copper-64 activity

long lived element. This enables the shorter lived element
to reach a higher proportion of its saturation activity than
the long lived element, thereby facilitating the detection
of the short lived element. Of course, if the saturation
activity of the longer lived activity is many times larger
than that of the shorter lived activity, even a small fraction
of it may mask the other. The magnesium oxide matrix being
99.99% pure will have a saturation magnesium activity of 100
to 1000 times greater than the maximum amount of titanium or
calcium that might be present. Thus even a short irradiation
favoring the titanium or calcium will result in a high
magnesium activity which will tend to mask the titanium peak
and produce a high analyzer dead time reducing the sensi-
tivity to calcium.

To check the possibility of detecting short half life
elements, a magnesium oxide sample was irradiated for 30 sec
in R-6 of the ALRR facility. Counting was started 4 min
after the end of the irradiation on the Ge(Li) detector RIDL
1600 channel analyzer system. Four min was the minimum time
required for the necessary Health Physics monitoring and
transport of the sample to the detector. The results, shown
in Fig. 19, indicate no activities other than the magnesium
of the matrix. From this experiment it was concluded that
it was not possible with the present experimental arrangement
to identify trace impurities whose activities were on the same
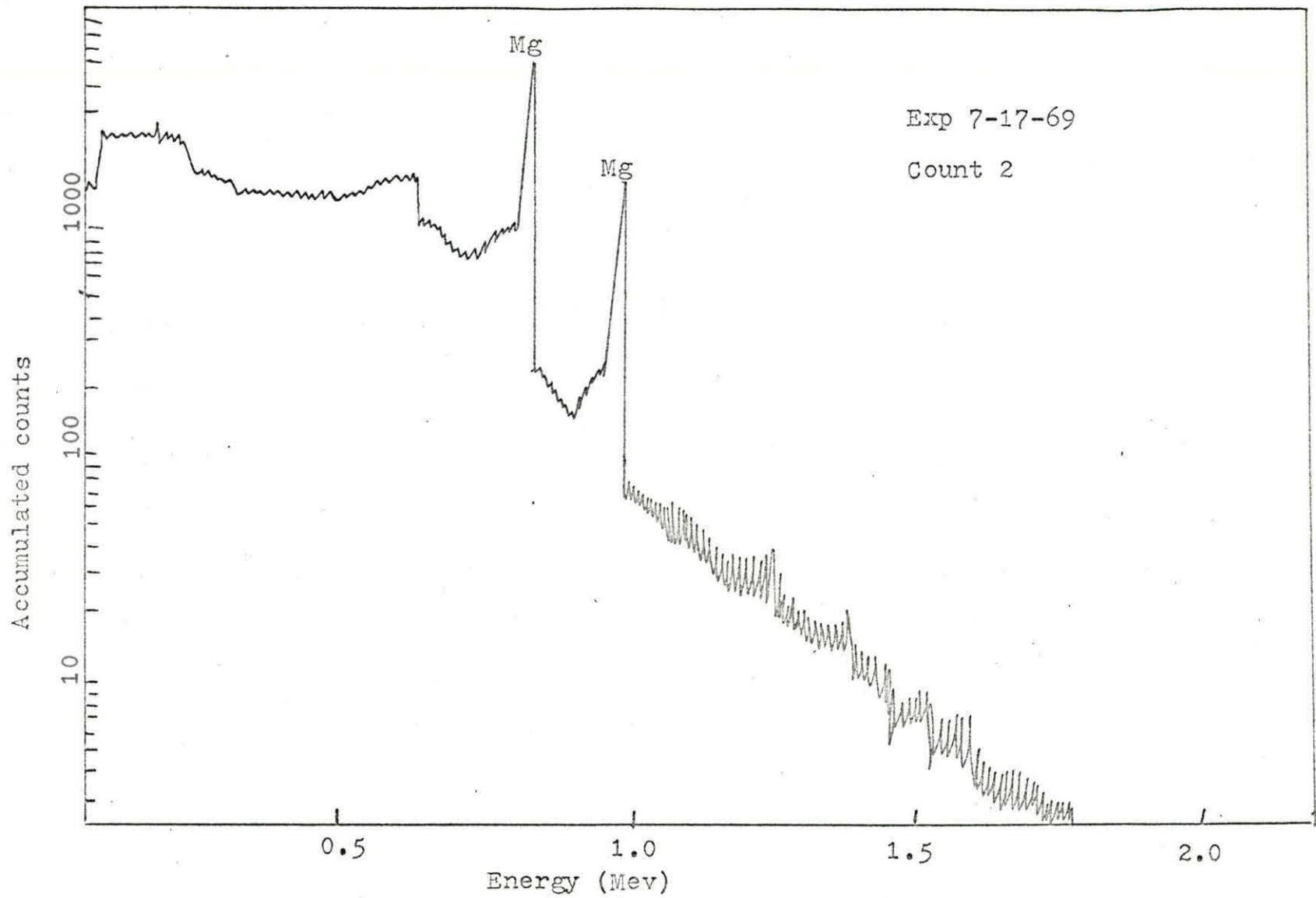
Fig. 19. Spectrum showing short lived activities in an MgO crystal

order of magnitude as the magnesium of the matrix. This ruled out all the isotopes with (n,γ) reactions listed in Table 4. Those with fast reactions were previously ruled out by the strong activity produced by the $^{24}Mg(n,p)^{24}Na$ reaction.

A possible exception was calcium whose full-energy peaks, as listed in Table 4, fall at 3.10, 4.10, and 4.63 Mev, well above the magnesium peaks. Because the Ge(Li) detector has an extremely low efficiency at high energies, the NaI detector was chosen to test this possibility. Separate irradiations of 15 min each were conducted in the UTR-10 rabbit at a flux of 6×10^{10} n/cm^2sec for 3.0×10^{-2} and 1×10^{-5} gm calcium samples and a 0.283 gm magnesium oxide crystal. Counting was done within 4 min of the end of each irradiation and yielded a characteristic calcium spectrum for only the 3.0×10^{-2} gm sample. Furthermore, the magnesium oxide showed a high activity which resulted in a high analyzer dead time. While the detection of calcium in a magnesium oxide matrix by activation analysis looks good in theory, it was concluded that it could not be accomplished with the present equipment and techniques.

Analysis for Specific Elements

With the exception of the check for calcium, the analysis of irradiations has been general. The method has been to analyze all activities in spectra from experiments emphasizing

the long, short, or intermediate half-life activities. This
analysis thus far has identified scandium and cobalt plus
the following elements listed on the emission spectrometric
analysis: chromium, copper, iron, and manganese and has not
detected barium, cesium, molybdeum, nickel, silicon, titanium
and calcium. Of these, calcium and titanium have only short
lived activities and cannot be detected in the short lived
magnesium oxide matrix. Silicon has several fast reactions
which are ruled out due to the high activity $^{24}Mg(n,p)^{24}Na$
reaction. In addition, no trace of the 1.26 Mev gamma ray
activity characteristic of the (n,γ) reaction of silicon has
been noted on any of the intermediate half-life spectra. The
relevant nuclear characteristics of silicon are given in
Table 5.

Normalization calculations with the manganese-56 peaks
shown in Fig. 20 indicate that to have a statistically
significant silicon full-energy peak at 1.26 Mev, a concen-
tration of 1×10^4 ppm of silicon must be present in the
magnesium oxide crystal. While a somewhat higher sensitivity
may be achieved by an irradiation in a higher flux location
than that used for the manganese determination, the inverse
relationship between the flux and the cadmium ratio typical
of a nuclear reactor results in a lower cadmium ratio causing
the prohibitive $^{24}Mg(n,p)^{24}Na$ reaction.
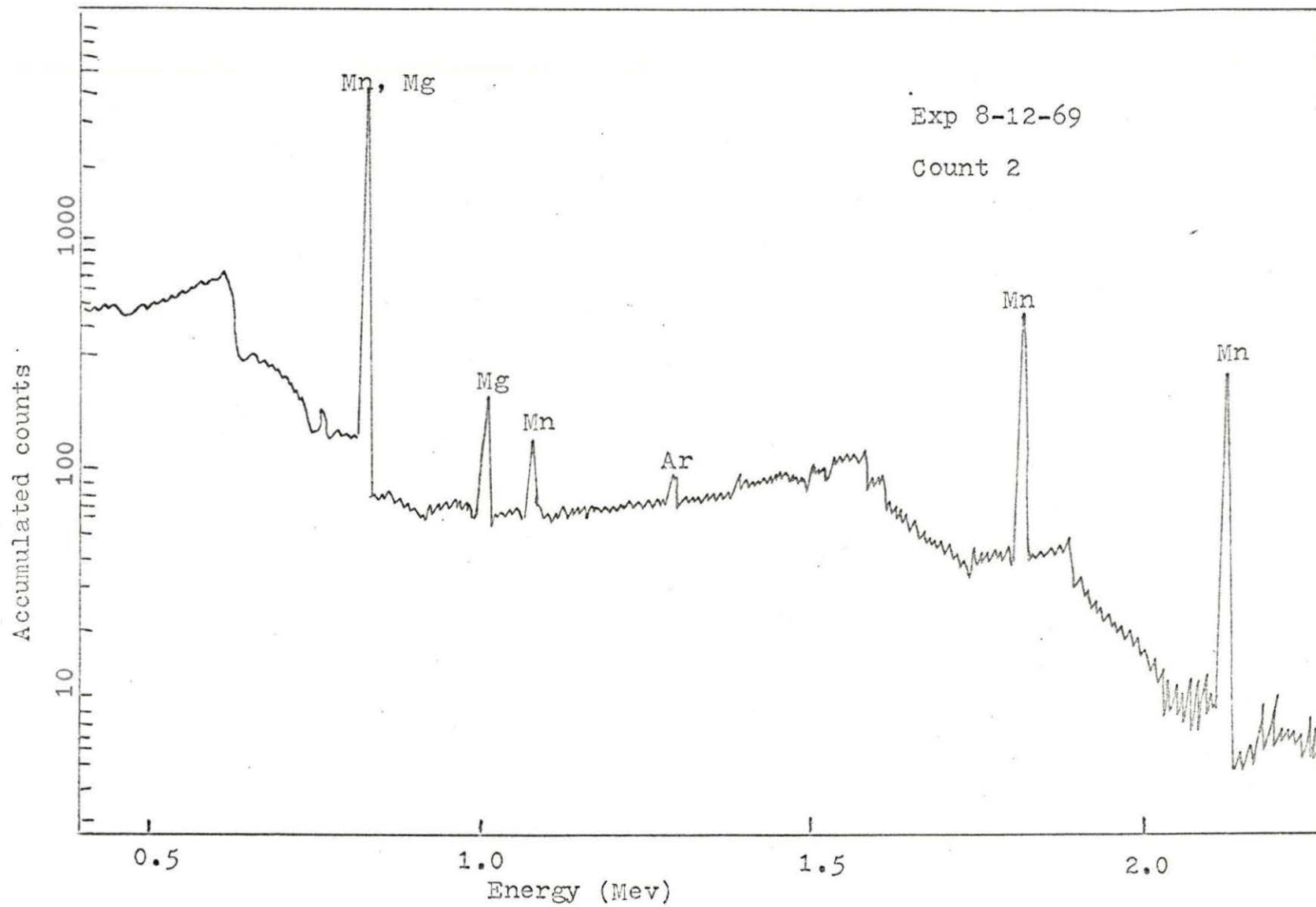
To test the sensitivity of this analysis for nickel,

Fig. 20. Spectrum showing manganese-56 activity in an MgO crystal

cesium and barium, a standard of approximately 1×10^{-6} gm of each was irradiated along with a 0.227 gm magnesium oxide crystal at a flux of 6×10^{10} n/cm^{2}sec, cadmium ratio > 1000, for 3 hr. These additions represent an impurity concentration of approximately 4 ppm. Analysis of the spectra showed no activities indicating the presence of these elements in either the standard or the crystal. These results, plus a matrix normalization calculation determining the sensitivity of this analysis for the above elements from the manganese-56 that had already been detected lead to the conclusion that either these elements were not present or were in concentrations less than those listed in Table 7.

This same procedure was repeated for molybdenum and barium using a flux of 3.4×10^{13} n/cm^{2}sec and cadium ratio < 20. A weak 2.75 day molybdenum activity appeared in the spectrum of the standard but none was present in that of the magnesium oxide crystal. This indicated that the molybdenum if present in the crystal was at a concentration of < 4 ppm. Barium was not detected in either the spectrum of the standard or the crystal. Therefore, if present it is assumed to be in a concentration of less than 2 ppm as indicated in Table 7. The apparent discrepancy between the calculated detection limit of 2 ppm and the lack of detection of a 4 ppm standard is not surprising. The sensitivities are only approximate due to uncertainties in the tabulated

Table 7.   Approximate sensitivities for techniques described

Element	Isotope	Half-life of product	Specific activity (dpm/ug)	Normalized sensitivity
Nickel	^{69}Ni	2.56 hr	2.8×10^3	38 ppm[a]
Cesium	^{133}Cs	2.9 hr	1×10^3	48 ppm[a]
Barium	^{138}Ba	1.42 hr	3.7×10^4	2 ppm[a]
Molybdenum	^{98}Mo	2.75 days	4.4×10^2	< 1 ppm[b]

[a] 3 hr at 6×10^{10} n/cm^{2}sec.

[b] 3 hr at 3.4×10^{10} n/cm^{2}sec.

specific activities and the detector efficiency. It is
suggested that further experimental work in assigning
detection limits be done.

Comparison of Results with Emission Spectrometric Analysis

This qualitative activation analysis has detected
copper, manganese, chromium, scandium, iron, and cobalt.
All of these are listed in the emission spectroscopic
analysis shown in Fig. 14 except for scandium. In addition,
barium, calcium, cesium, molybdenum, nickel, silicon, and
titanium are listed. To resolve the difference, an associ-

ate chemist[1] of the Analytical Services Group II of Ames
Lab was consulted. The following conclusions were reached:

1) The barium, cesium, molybdenum, nickel, silicon
and titanium, if present, were in such small quantities that
they could not be positively identified with the emission
spectroscope, although weak lines which may have been inter-
ference did appear at characteristic locations for these
elements. Since this activation analysis was shown not to
be sensitive to approximately 1 ug or 4 ppm concentrations
of these elements, no discrepancy remained between it on the
emission spectroscopic analysis. Neither gave a positive
indication of the presence or absence of these elements.

2) The calcium was positively identified by the spec-
troscopic analysis, but because of its short half-life it
could not be identified in the magnesium oxide matrix by
activation analysis. In addition, the high energies of the
full-energy peaks coupled with the low detector efficiency
at these energies create a low sensitivity for calcium.

3) The scandium did not appear in the emission spec-
troscopic analysis which has a sensitivity for scandium of
about 20 ppm. The activation analysis positively identified
scandium and a later quantitative analysis indicates it is
present in a concentration of 0.21ppm (Table 11).

---

[1]DeKalb, Edward L., 8 Research, Ames Lab, Ames, Iowa.
Qualitative analysis of magnesium oxide by emission spec-
troscopy. Private communication. 1969.

Comparison of the Ge(Li) and NaI(Tl) Detector Systems

This analysis parallels that of Lee (30) except here the high resolution of the Ge(Li) detector system (4.5 Kev at 1333 Kev) is used to resolve the scandium-46, iron-59, and cobalt-60 activities. Previously the poor resolution of the NaI(Tl) detector (7% at 0.662 Mev) had dictated the use of separation techniques as discussed by Lee. In addition, because the scandium peak is much more pronounced than the iron peak and has a longer half-life, the very presence of iron had to be suggested by some other means so that a separation and positive identification could be made. While the cobalt-60 activity with its half-life of 5 yr could have been determined after a prolonged delay by waiting for the 85 day scandium-46 to decay the Ge(Li) detector system permits an identification in less than 10 days. Furthermore, because the Ge(Li) detector system is able to resolve peaks to a greater degree, the possibility of introducing an error in the qualitative analysis due to the summation of the activities of several isotopes is reduced.

The advantages of the Ge(Li) detector system are demonstrated in Fig. 21 where a superposition of two spectra of the same magnesium oxide crystal is shown, one taken on the Ge(Li) and the other on the NaI(Tl) detector system. While the Ge(Li) detector system is less efficient than the NaI(Tl), dictating a longer counting period to obtain a sufficient number of counts, this was judged more of an
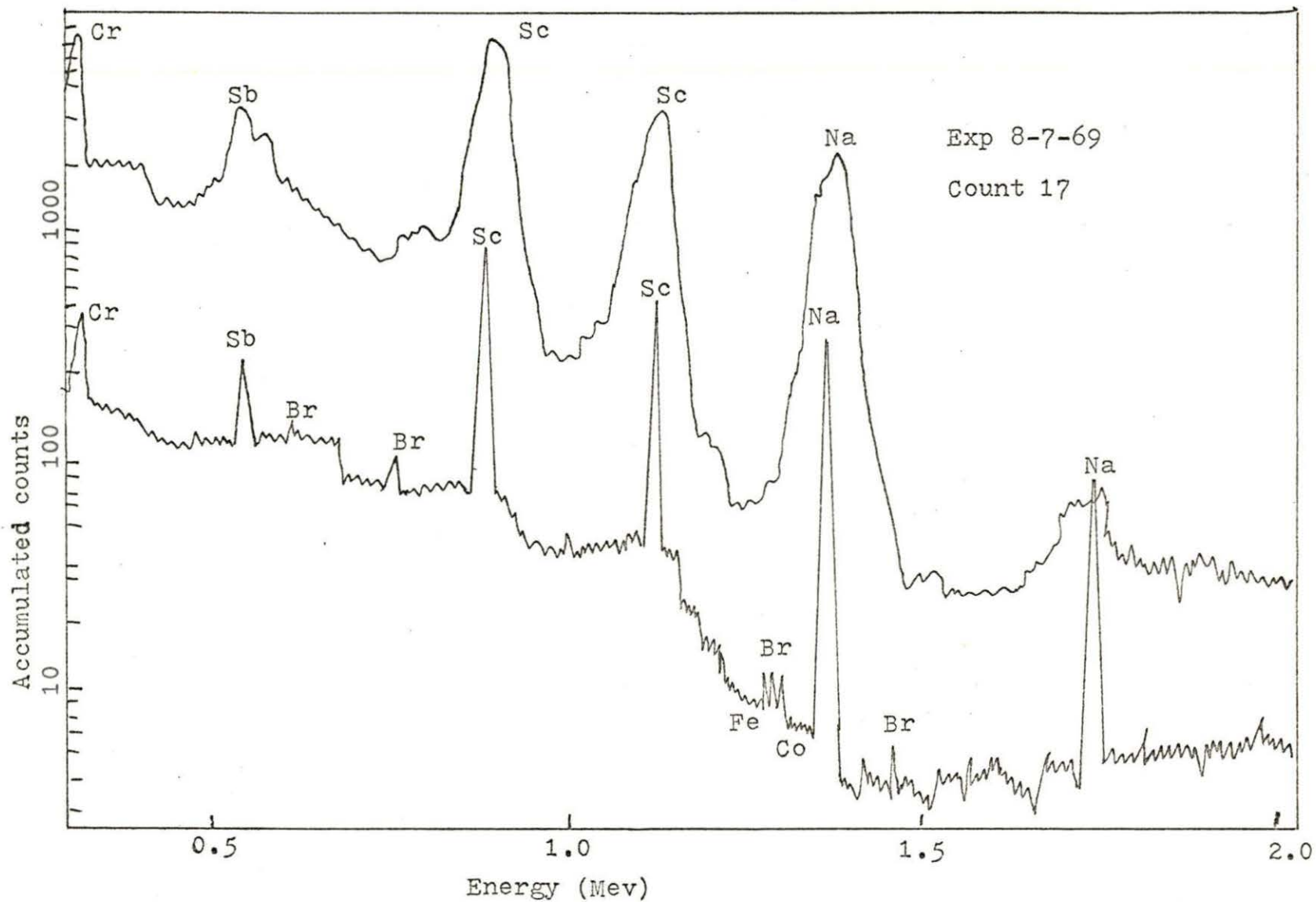
Fig. 21. Spectra of MgO crystal comparing the Ge(Li) and NaI(Tl) detectors

inconvenience than a shortcoming.

It was concluded that Ge(Li) detector, was in most cases superior to the NaI for activation analysis work. The small disadvantage of the slightly lower efficiency of the Ge(Li) detector is usually outweighed by the advantage of the increased resolution. One case in which the NaI is better occurs when the peaks are well separated and sensitivity is a problem.

CHAPTER V. QUANTITATIVE ANALYSIS

The comparison method was chosen for the quantitative
analysis for reasons discussed in Chapter II. The method
as noted before requires the preparation of standards for
the elements present in the sample; simultaneous irradiation
of the sample and standards; and in addition, the spectra
must be taken under identical conditions, i.e., same equip-
ment, calibration, and counting geometry.

If the above conditions are met, the weight of the
element of interest may be determined from the following
equation:

$$wt_u = \frac{A_u}{A_s} \, wt_s \, e^{-\lambda \Delta t} \qquad (23)$$

in which

wt_u = unknown weight,

wt_s = standard weight,

A_u = full-energy peak area of unknown,

A_s = full-energy area of standard,

$e^{-\lambda \Delta t}$ = decay correction for the difference in decay
times,

Δt = the difference in decay time between counting
the standard and the unknown,

λ = decay constant.

A more rigorous equation developed in Chapter II includes
the dependence on the other possible experimental variables and
assigns an uncertainty to the calculated weight. An

example showing its application is given in the error analysis
in Chapter VI. To eliminate the tedious calculations and
reduce the possibility of human errors, the mass determina-
tion and uncertainty calculations as shown in the error
analysis have been written into a computer program for the
IBM 360/65.

Preparation of Standards

.For the greatest accuracy, the comparitor standards
should contain the same weight of the element of interest as
the sample being analyzed. Since these weights were not
known, an arbitrary value of 10 ppm was chosen. With the
typical crystal weight being 0.3 gm, this yielded a prelimi-
nary standard weight of 3.3×10^{-6} gm. An analysis using
this set of standards produced better estimates for a final
set of standards. To produce comparitor standards of this
magnitude, dissolution and dilution micro-chemistry techniques
were used.

Volume measurements were done in Pyrex volumetric
flasks and with Pyrex micro-pipets. Weighing was done on
either a Gram-atic Balance (Ames Lab #10188) or a Cahn
Electro-Balance (Ames Lab #11302). Since weighing out an
exact, predetermined amount is extremely tedious, the pre-
determined amounts were approximated within a factor of 2
on a clean slip of weighing paper. The paper and standard
materials were weighed together, the material was poured

into a labeled volumetric flask, and the paper was reweighed. The difference between the two weights was recorded as the weight used and is presented in Tables 8, 9, and 10. When metals were to be dissolved to produce standards, they were first etched to remove any surface contamination which may have been introduced by handling.

To produce a manganese standard, a portion of MnO_2 was weighed out and dissolved in HNO_3 with the aid of H_2O_2, an oxidizing agent. This solution was diluted to 1000 ml with distilled H_2O and a part of it was micropipetted into a pre-cleaned polyethylene capsule identical to the ones used to encapsulate the MgO samples. Before pipetting, the solution was shaken vigorously for several minutes to insure homogeny. The pipetting technique included wiping the outside of the pipet dry before delivery and rinsing the pipet three times, each time with a premeasured drop of distilled water of the same volume as the pipet. This insured complete delivery of the standard solution. The contents of the polyethylene capsules were then evaporated to dryness under an infrared lamp. This drying was done under a plexiglass plate to insure that dust from the room would not settle into the capsules during the 4 to 6 hrs involved. After the standard was dried, the capsule was closed and sealed in a polyethylene envelope which was inserted into a larger capsule and irradiated along with the MgO crystal. It was found that the

Table 8. Specifications of preliminary comparison standards

Element	Form	Solvent	Weight (gm)	Volume (ml)	λ in std	wt of element in std (gm)
Scandium	metal	nitric acid	0.0046	1000	100	4.6×10^{-7}
Cobalt	metal	nitric acid	0.0128	1000	100	1.28×10^{-6}
Iron	metal	nitric acid	0.0035	1000	100	3.5×10^{-7}
Chromium	CrO_3	nitric acid	0.0154	1000	10	1.54×10^{-7}
Manganese	MnO_2	nitric acid and hydrogen peroxide	0.0225	1000	100	2.25×10^{-6}

Table 9. Specifications of the comparison standards for analysis 1

Element	Form	Solvent	Weight (gm)	Volume (ml)	λ in std	wt of element in std (gm)
Scandium	metal	nitric acid	0.0076	1000	100	7.6×10^{-7}
Cobalt	metal	nitric acid	0.0041	1000	10	4.1×10^{-8}
Iron	metal	nitric acid	0.0106	1000	100	1.06×10^{-6}
Chromium	CrO_3	nitric acid	0.0011	1000	10	1.1×10^{-7}
Manganese	MnO_2	nitric acid and hydrogen peroxide	0.0191	1000	100	1.9×10^{-6}

Table 10. Specifications of comparison standards for analysis 2

Element	Form	Solvent	Weight (gm)	Volume (ml)	λ in std	wt of element in std (gm)
Scandium	metal	nitric acid	0.0015	10000	10	1.5×10^{-9}
Cobalt	metal	nitric acid	0.0021	1000	20	4.2×10^{-8}
Iron	metal	nitric acid	0.0205	500	200	8.2×10^{-5}
Chromium	CrO_3	nitric acid	0.0013	100	100	1.3×10^{-5}
Manganese	MnO_2	nitric acid and hydrogen peroxide	0.0235	1000	100	2.3×10^{-6}
Copper	CuO	nitric acid	0.0235	100	10	2.3×10^{-6}

count rate correlation between identical standards pipetted using a non-wiping, non-premeasured rinse technique was approximately 90% while the correlation using the rigorous technique described above was approximately 99%. Similar techniques were used to prepare the other standards used in this analysis.

For the preliminary set of standards, each standard was pipetted into a separate capsule, but for the final set all of the standard solutions were pipetted into the same capsule. This was done in order to provide a standard which would approximate the MgO sample as closely as possible with respect to its activation characteristics and in addition to reduce the number of separate samples to be counted.

The standards materials, their amounts, and the solvents used in the preliminary and two final sets of standards are presented in Tables 8, 9, and 10. The sources and analysis of the metals, compounds, and reagents involved are given in Appendix C.

Irradiation of Samples and Standards

Irradiations for the quantitative analysis were done at the ALRR facility. To compensate for the flux gradient in the reactor, a standard was placed on either end of the sample as shown in Fig. 13. The position and alignment were maintained by the large polyethylene capsule which had an

inside diameter slightly greater than the outside diameter
of the samples and a length equal to three samples. Poly-
ethylene packing cut from a clean disposable glove was used
to keep the crystal centered in the bottom of its capsule
during irradiation. The packing was removed prior to
counting so that any contribution from the containers
should be the same for all three capsules. The distances
between the inside bottoms of the two capsules and between
the inside bottom of capsule two and the center of the
crystal were measured so that a flux gradient correction
could be made. A sample calculation is included in Chapter
VI.

The irradiation necessary for the search for manganese
and copper was done in location TV1 (flux = 6 x 10^{10} n/cm^2
sec, cadmium ratio 1000) to eliminate interference from the
^{56}Fe(n,p)^{56}Mn reaction, see Table 5. After counting and
waiting for the manganese and copper activities to decay,
the same crystal was again irradiated, this time with the
composite iron, scandium, chromium, and cobalt standards
placed on either end of the sample as shown in Fig. 13.
This three hour irradiation was carried out in R-3 (flux =
3.0 x 10^{13} n/cm^{2}sec, cadmium ratio < 20).

Activity Measurements

The Ge(Li) detector analyser systems described in
Chapter III were used for these measurements. For the

manganese determinations, counting was started approximately one hour after irradiation while for the copper approximately an eight hour delay was used. These times permitted, in the first case, the extremely high activity of matrix magnesium to decay while, in the second case, it permitted the manganese activity to subside. This reduced the analyser dead time and the background of the spectrum enhancing the contours in the full-energy peaks areas. The samples were rotated during counting to remove geometric differences as discussed in Chapter III.

The measurement of chromium, scandium, iron, and cobalt activities was done after a minimum of seven days delay. This permitted the high sodium activity from the $^{24}Mg(n,p)^{24}Na$ reaction to decay.

In both of the above cases, counting was continued until either 4000 counts had accumulated in the center channel of the peak of interest or the available time had elapsed. Because the specific activities of the iron and cobalt are so low and the efficiency of the Ge(Li) detector is only about 3.5% of that of a NaI(Tl) detector in the energy range of the cobalt and iron activities, counting periods of up to six hours were needed.

Results

The photon energies associated with the experimentally measured full-energy peaks were obtained from the computer

program ICPEAX (Appendix A). After inspecting the plots to insure that the peaks appeared "normal" with no obvious interferences, the areas provided by the program were introduced into Equations 15-22 of Chapter II. The manner in which data is handled is shown in Chapter VI. These calculations done with the IBM 360/65 computer, give the concentrations of impurities present in ppm. The results of the analysis together with a repeat of the analysis to establish reproducibility are given in Table 11.

An error caused the standards for the Cr, Fe, and Co in analysis 1 to be too small so that the calculated values of these elements are only approximate. In analysis 2, no difficulties were encountered and a better set of values resulted. The agreement between the Mn and Sc values for analyses 1 and 2 increase the contents in the second analysis. The uncertainties in the Fe and Co in analysis 2 could be improved with further work.

Table 11.   Results obtained for impurities in a magnesium
            oxide crystal

	ppm	Error
Analysis 1		
Mn	6.3	± 1.1
Cr	5	-
Cu	-	-
Fe	17	-
Co	1	-
Sc	0.21	± 0.01
Analysis 2		
Mn	5.9	± 0.3
Cr	9.26	± 0.57
Cu	0.73	± 0.07
Fe	94	± 64
Co	0.14	± 0.07
Sc	0.21	± 0.03

CHAPTER VI. ERROR ANALYSIS AND SAMPLE CALCULATION

A preliminary error analysis considering all the experimental procedures that might introduce errors or uncertainties in the qualitative or quantitative analysis was carried out prior to the experimental phase of this work. The uncertainties associated with each of the experimental procedures, combined using propagation of errors theory, pointed out those procedures in which the uncertainties are most significant. The preliminary error analysis indicated that the most significant uncertainty would be that associated with the determination of the full-energy peak area.

To decrease this uncertainty in subsequent work, irradiation and counting times were increased so that the accumulated count in the center channel of a full-energy peak was at least 400 and preferably 4000-5000 counts. In addition a computer program, ICPEAX, was used to find full-energy peak areas. While the program may or may not be more accurate than hand techniques it is more consistent since it does remove human variations. Furthermore, since the comparison technique is used, consistent errors tend to cancel so the accuracy of the analysis is enhanced.

Upon completion of the experimental work, the error analysis was repeated in detail as given in this chapter. There are certain errors common to both qualitative and

quantitative instrumental neutron activation analysis. In qualitative analysis, a binary decision is involved; either an element is or is not detected. This decision may be confused by various factors including: 1) interfering gamma rays at the same, or approximately the same, energy, 2) incorrect calibration of, or drift in, the calibration of the analyser resulting in the assignment of incorrect energies to, and, therefore, incorrect identification of the characteristic full-energy peaks and 3) epithermal reactions which may produce activities in addition to, or in competition with, the desired (n, γ) reactions.

The probability that two or more gamma rays interfered and thus introduced an error in this analysis was considered small for the following reasons:

First, a calibration check of seven separate counts, acquired over a 6 hr period, showed that ICPEAX, working with the data obtained with the ORTEC Ge(Li) detector - Nuclear Data analyser system described in Chapter II, assigned energies to the full-energy peaks with an average error of ± 0.47 Kev from the tabulated values. The largest deviation was - 2.6 Kev and the deviations occurring most often were - 0.2 and + 0.3 Kev.

Second, the plots obtained with this calibration check showed that full-energy peaks 10 Kev apart are clearly separated and that peaks only 5 Kev apart could be resolved.

Third, using the data listed in Heath (18), a check was made for all nuclides having gamma ray activities 5 Kev above and below the identified peaks. Each of these nuclides was methodically eliminated by differences in either or both the characteristic spectrum and the half-life.

Epithermal reactions which may occur and interfere with the desired (n, γ) reactions, as listed by Lee (30), are presented in Table 12.

Table 12. Summary of possible interference reactions

Element sought	Competition reaction	Absorption cross section (mb)
Scandium	$^{46}Ti(n,p)^{46}Sc$	4.1
Chromium	$^{54}Fe(n,\alpha)^{51}Cr$	0.37
Manganese	$^{56}Fe(n,p)^{56}Mn$	1.10
	$^{59}Co(n,\alpha)^{56}Mn$	35
Iron	$^{59}Co(n,p)^{59}Fe$	22
	$^{60}Ni(n,\alpha)^{57}Fe$	-
Cobalt	$^{63}Cu(n,\alpha)^{60}Co$	-
	$^{60}Ni(n,p)^{60}Co$	5

The error introduced by the ^{46}Ti(n,p)^{46}Sc reaction is negligible because 1) the titanium if present at all, will be only in trace amounts, 2) the abundance of the titanium-46 isotope is only 7.99% and 3) the cross section is small. The same comments apply to the ^{60}Ni(n,α)^{57}Fe and ^{60}Ni(n,p)^{60}Co reactions except the isotopic abundance of nickel-60 is 26%.

While the iron is the matrix impurity expected to have the greatest concentration, the abundance of the iron-54 isotope is only 5.4%. This coupled with the small cross section for the ^{54}Fe(n,α)^{51}Cr reaction eliminates it as a matter of concern. The possible interference from epithermal reactions producing manganese-56 activity was eliminated by carrying out the manganese determination irradiations in as "thermal" a flux as possible, i.e., R_{cd} greater than 1000. The cross section of the remaining ^{63}Cu(n,α)^{60}Co reaction is only 11.4 mb for fast neutrons eliminating it as a possible interference.

Other qualitative sources of error include contamination which may occur during sample preparation and handling and the possibility that constituents of the irradiation capsule might be considered to be impurities in the actual sample. Etching the sample before irradiation and analysis of the acid used in the etching process eliminated the first possibility while the irradiation and analysis of an empty capsule made possible the elimination of the second. (See Fig. 22)
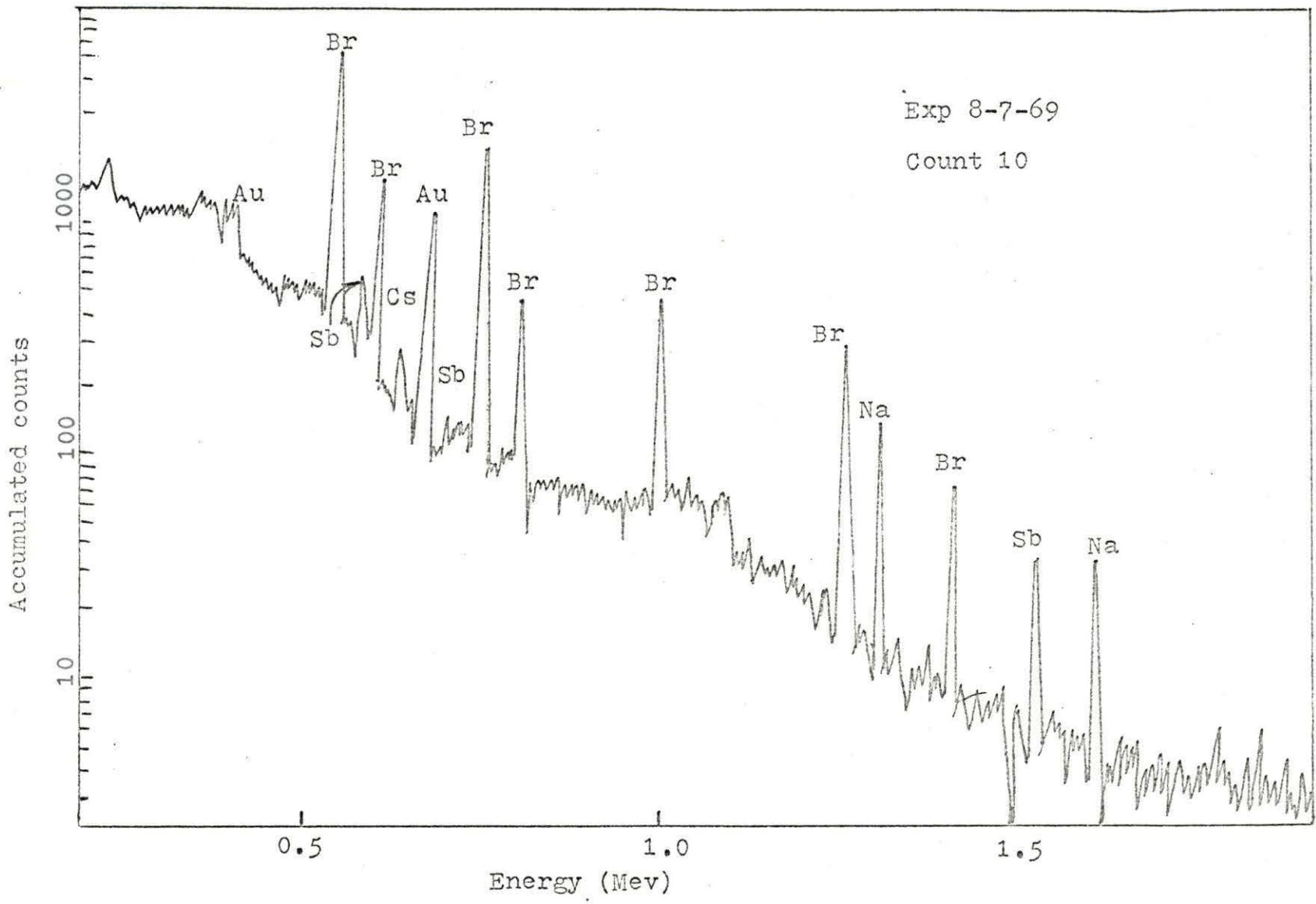
Fig. 22. Spectrum of empty polyethylene capsule

The largest uncertainty in the quantitative analysis occurs when analysing an element whose concentration approaches the limits of the sensitivity of the method which occurs when the standard deviation of the channel counts approaches the height of the full-energy peak above the background.

The error or uncertainty in the quantitative analysis may be found by applying propagation of errors theory to each of the terms in Equation 24.

$$m_u = \frac{f_s A_u \Theta_s m_s \emptyset_s S_s e^{-\lambda_s t d_s} (1-e^{-\lambda_s t c_u})}{A_s \Theta_u f_u \emptyset_u S_u e^{-\lambda_u t d_u} (1-e^{-\lambda_u t c_u})} \qquad (24)$$

The meanings of those terms not immediately obvious may be found by referring to Equation 3 of Chapter II. The uncertainties considered in this analysis are listed in Table 13.

Although the experimenter would like to reduce the uncertainties in each term to values as small as possible, it is clear that the only effective effort is that devoted to reducing the magnitude of the major contributions. For purposes of illustration, all contributions to the uncertainty in the determination of the manganese impurity in the magnesium oxide crystal are discussed in detail in the following analysis.

While analyzing the techniques used in the preparation of a comparitor standard of a known weight as discussed in the

Table 13.   Tabulation of uncertainties in the quantitative
            analysis

I.   Uncertainties in weight of standard

   A.   Purity of standard material

   B.   Weighing of standard material

   C.   Volume dilution

   D.   Pipetting of standard into capsule

   E.   Homogeny of standard solution

II.   Uncertainty in purity of standard samples, i.e.,
      possibility of introducing a confusing reaction

III.   Uncertainty in purity of reagents, cleaning fluids
       and solvents

IV.   Uncertainty in cleanliness of glassware

V.   Uncertainty in weight of sample analysed

VI.   Uncertainty in flux ratio between locations occupied
      by standard and sample

VII.   Uncertainty in self-shielding ratio of standard to
       sample

VIII.   Uncertainty related to counting geometry

IX.   Uncertainty in counting period

X.   Uncertainty in decay time

XI.   Uncertainty in half-life

XII.   Uncertainty in full-energy peak area

XIII.   Uncertainties peculiar to a specific detector
        analyser and data handling system

quantitative analysis, the uncertainties listed in Table 13
are considered. The standard material is never 100% pure.
Usually the best that can be expected from an analysed
reagent is 99.99% purity with an analysis stating the
impurities and their concentrations. Related to the purity
of the standard is its form. In the case of manganese, the
compound manganese dioxide was used. Since manganese has a
molecular weight of 54.938 $\pm$ 0.0005 and the manganese
dioxide has a molecular weight of 86.94 $\pm$ 0.005, the actual
manganese used will be the ratio of the molecular weights
times the purity times the mass used. The uncertainties in
the molecular weights are assumed to be one-half of the last
significant figure.

The weighing was done using a Gram-atic balance (serial
#1-910) whose calibration was checked by the experimenter
with a set of calibration weights from a Cahn electrobalance
(Ames Lab #11302). The balance, which is graduated down to
0.0001 gm, was found to weigh the calibration weights to
$\pm$0.0001 gm of their imprinted values in repetitive trials.

The samples were weighed by the difference technique.
To insure that only the amount of standard used was recorded,
the weighing paper and standard were weighed first, the
standard was poured from it into a volumetric flask and
the paper and the residual standard on it were reweighed.
For the manganese standard, 36.6 mg of manganese dioxide was

used. When the ratio of the molecular weights and the purity of the manganese dioxide are applied to this, the weight of the manganese in the standard and its uncertainty becomes

$$(wt \pm \Delta wt)_{MnO_2} = (wt_t - wt_p) \pm \sqrt{(\Delta wt_t)^2 + (\Delta wt_p)^2}$$

(25)

$$= 0.0366 \pm \sqrt{(0.001)^2 + (0.001)^2}$$

$$wt \pm \Delta wt = (36.6 \pm 0.14) \times 10^{-4} \text{ gm}$$

$$(wt \pm \Delta wt)_{Mn} = \frac{(wt_{MnO_2})(mw)_{Mn}(purity)}{(mw_{MnO_2})}\left[1 \pm \sqrt{\left(\frac{\Delta wt}{wt}\right)^2 + \left(\frac{\Delta mw}{mw}\right)^2_{Mn}} \right.$$

$$\left. + \left(\frac{\Delta mw}{mw}\right)^2_{MnO_2} + \left(\frac{\Delta purity}{purity}\right)^2 \right]$$

(26)

$$= \frac{(0.0366)(54.938)(0.9999)}{(86.94)}\left[1 \pm \sqrt{\left(\frac{0.00014}{0.0366}\right)^2} \right.$$

$$\left. + \left(\frac{0.0005}{54.938}\right)^2 + \left(\frac{0.005}{86.94}\right)^2 + \left(\frac{0.005}{99.99}\right)^2 \right]$$

$$= 0.0232\left[1 \pm \sqrt{1.5 \times 10^{-7} + 8.3 \times 10^{-11}} \right.$$

$$\left. + 1.9 \times 10^{-9} + 2.5 \times 10^{-10} \right]$$

$$(wt \pm \Delta wt)_{Mn} = 0.0232 \pm 0.0001 \text{ gm}$$

This mass of manganese in the form of manganese dioxide was dissolved in nitric acid with the help of hydrogen peroxide and then diluted with distilled water to 1000 $\pm$ 0.30 ml in a Pyrex volumetric flask. Care was taken to insure that the flask and its contents were at room temperature (an air conditioned 20° C) before the level of the solution in the flask was brought up to the calibration line. The analysis of the nitric acid and the hydrogen peroxide is given in Appendix C. In addition, approximately 250 λ of the distilled water was irradiated and analysed (Fig. 23). As a result of these analyses, it was judged that the distilled water, the nitric acid and the hydrogen peroxide did not contribute significantly to any activity which could be mistaken for the standard and thereby introduce an error.

The actual standard was produced by pipetting 100 λ of this solution into a polyethylene capsule. Kimax micropipets with a published tolerance of 0.3% at 20° C were used (26). Since this is the volume contained and not delivered, a careful wipe and triple rinse technique described in Chapter V insured that the total volume contained was delivered. To allow for possible human errors, a value of 1% was assigned to the pipetting uncertainty.

To insure that solutions were homogenous, first a check was made for any obvious precipitate. If any was
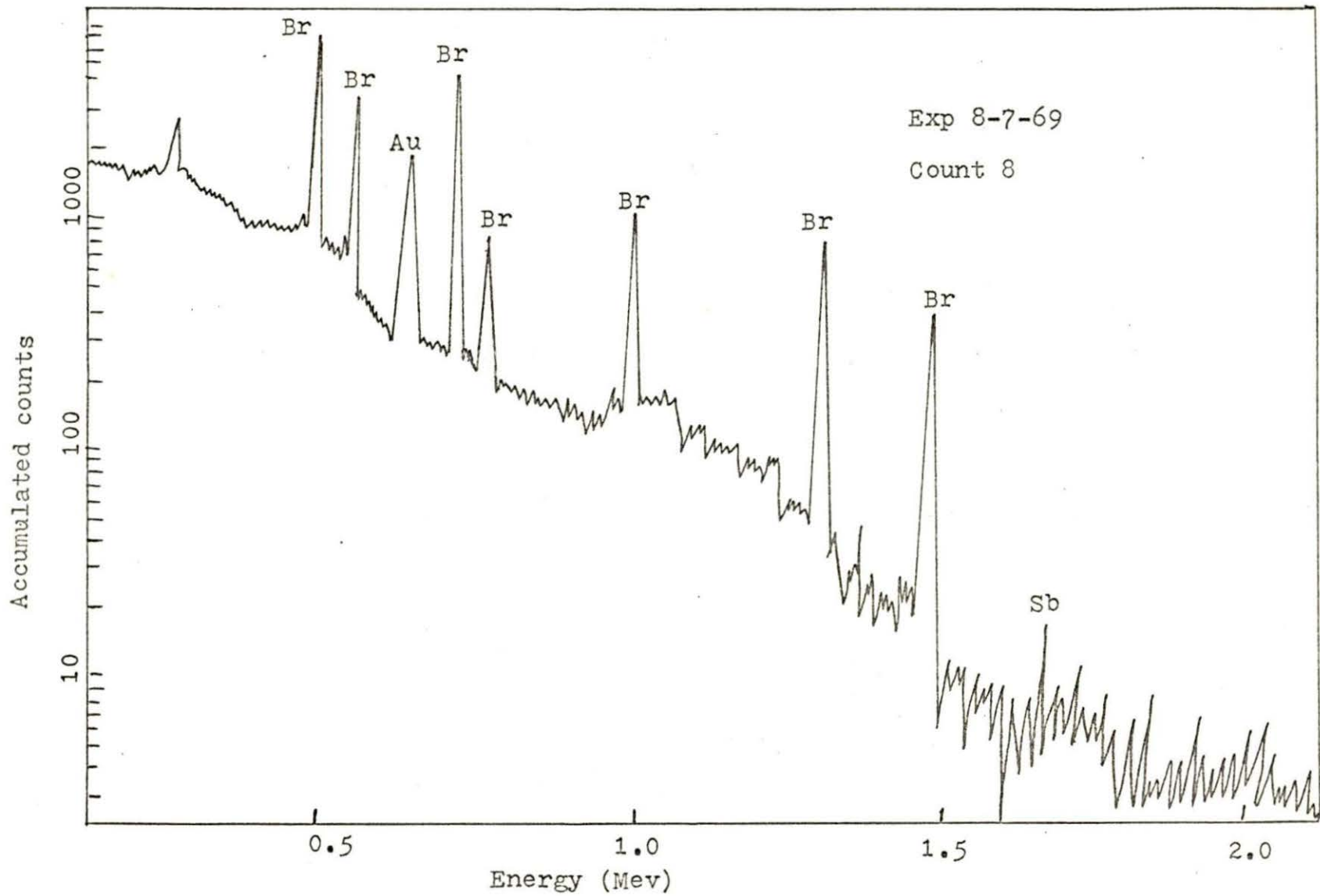
Fig. 23. Spectrum of distilled H_2O irradiated and counted in polyethylene capsule

found, a different compound and/or reagent was used to insure complete dissolution of the standard material. Second, all solutions were shaken well prior to use.

The dilution and micro-pipetting described yield a standard with the following weight and uncertainty

$$(wt \pm \Delta wt)_{std} =$$

$$\frac{wt_{Mn} \, vol_2}{vol_1} \left[1 \pm \sqrt{\left(\frac{\Delta wt}{wt_{Mn}}\right)^2 + \left(\frac{\Delta vol_1}{vol_1}\right)^2 + \left(\frac{\Delta vol_2}{vol_2}\right)^2} \right] \quad (27)$$

$$= \frac{(0.0232)(0.100 \; ml)}{1000 \; ml} \left[1 \pm \sqrt{\left(\frac{0.0001}{0.0232}\right)^2 + \left(\frac{0.30}{1000}\right)^2 + \left(\frac{1}{100}\right)^2} \right]$$

$$= 2.32 \times 10^{-6} \left[1 \pm \sqrt{5 \times 10^{-5} + 9 \times 10^{-9} + 1 \times 10^{-4}} \right]$$

$$(wt \pm \Delta wt)_{std} = (2.32 \pm 0.09) \times 10^{-6} \; gm$$

While it may be argued that part of the standard might have been lost during the drying process, the amount lost was considered to be negligible, because the standards are nonvolatile and the drying or evaporation took place at a very slow rate. Precautions were also taken to insure that dust and particulate matter did not settle from the air and into the standards during the drying process. To further insure that no contamination that might produce gamma rays at the same energies as the standards took place, clean

polyethylene gloves were worn during encapsulation and
samples were handled only with a forceps freshly cleaned
in acetone.

The glassware used in this analysis was cleaned by
Ames Lab personnel using the following standard technique:
Items are first dipped in alcohol to remove any grease.
This is followed by a soaking period in a solution of hot
sulfuric and nitric acid which is then followed by a rinse
in tap water. The glassware is then inspected for any
stubborn deposits which are then removed by hand brushing
with "BABO" a commercial cleanser. All pieces are then
rinsed with distilled water and put on a rack to dry. This
procedure appeared to be satisfactory since no unusual
activity which might be attributed to contamination from
the glassware was noted.

The weight of the crystal and the uncertainty in the
weight are found in the same way as the standard yielding

$$(wt \pm \Delta wt)_{crystal} = 0.2421 \pm 0.00014 \text{ gm}$$

During an irradiation the number of parent nuclides
decreases as the products are formed. During a long
irradiation the number of parent nuclei may be reduced
enough to reduce the reaction rate and give an erroneous
quantitative analysis. Using a cross section of 13.3 b for
manganese, a maximum flux of 3.4×10^{13} n/cm^{2}sec and a maxi-
mum irradiation time of 3 hrs, the sample calculation which

follows shows the decrease in the number of parent nuclei

is not significant.

$$N = N_{org} (\sigma) (T) (\emptyset)$$

$$N = N_{org} (13.3 \times 10^{-24})(3.4 \times 10^{13})(3)(3600)$$

$$N = 4.8 \times 10^{-7} N_{org}$$

where

N = the decrease in number of parent nuclei,

N_{org} = the original number of parent nuclei.

Since the decrease is negligible, no uncertainty has been

calculated.

During irradiation the samples are adjacent to one

another as shown in Fig. 24, yet they may be exposed to
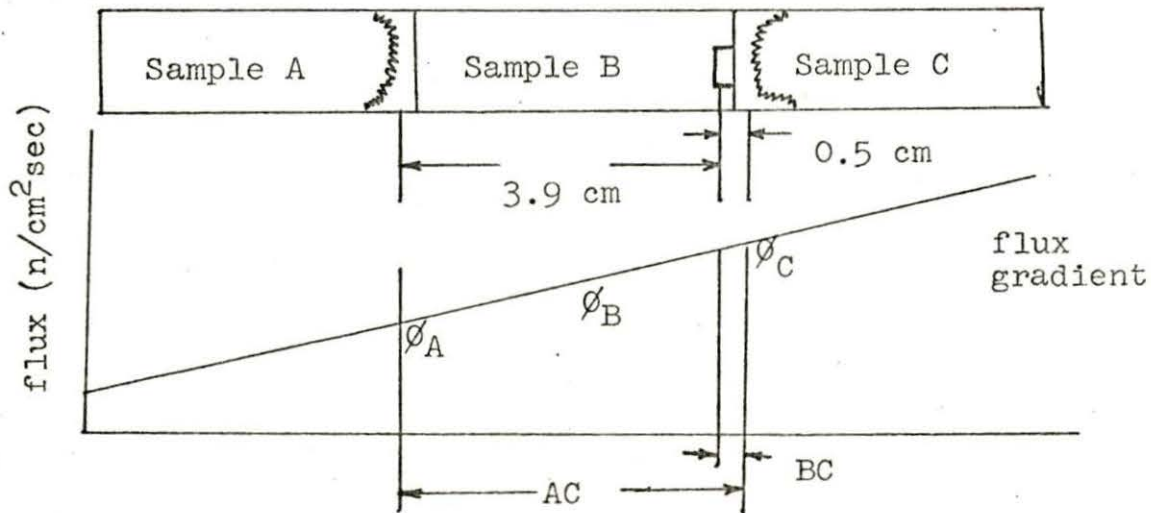
different fluxes due to spacial flux variations.

Fig. 24. Flux variation versus position

This variation was measured by placing "identical" standards A and C on either end of the magnesium oxide, sample B, during irradiation. The ratio of the flux at C to that at B

$$\phi_R = \frac{\phi_C}{\phi_B} \qquad (28)$$

may be found by measuring the same full-energy peak areas in standards A and C, and applying the ratios of the distances, to these peak areas to obtain a predicted peak area for sample B. Because the

$$(\text{full-energy peak area}) \propto (\text{activity}) \propto (\phi), \text{ the} \qquad (29)$$

flux ratio in Equation 28 may be found as

$$\phi_R = \frac{\phi_C}{\phi_B} = \frac{\overline{A}_C}{\overline{A}_B} \qquad (30)$$

where

$\overline{A}_C$ = full-energy peak area of sample C corrected for decay and counting times

and it can be readily shown that

$$\overline{A}_B = \overline{A}_A \frac{BC}{AC} + \overline{A}_C \frac{AB}{AC} \qquad (31)$$

Here

$\overline{A}_A$ = full-energy peak area of sample A corrected for decay and counting times,

$\dfrac{AB}{AC}$ = ratio of distance between samples A and B to the distance between samples A and C (See Fig. 24),

$\dfrac{BC}{AC}$ = ratio of distance between samples B and C to the distance between samples A and C.

The decay and counting corrections to the photo peak areas and their uncertainties, may be found by applying propagation of errors theory to

$$\text{Area} = m \, \phi \, e^{-\lambda t_d} \frac{\left(1 - e^{-\lambda t_c}\right)}{\lambda} \, K = A \tag{32}$$

where

t_d = decay time,

t_c = counting time

K = constant including saturation factor, detection efficiency, number of parent nuclei, etc.

The flux, ϕ, is proportional to the specific area which is given by

$$\overline{A} = \frac{A \lambda}{e^{-\lambda t_d}\left(1 - e^{-\lambda t_c}\right) m} \tag{33}$$

The specific area and its uncertainty is given by

$$\overline{A} \pm \Delta\overline{A} = \frac{A \lambda}{\left(1 - e^{-\lambda t_c}\right)\left(e^{-\lambda t_d}\right) m} \left[1 \pm \sqrt{\left(\frac{\Delta A}{A}\right)^2 + \left(\frac{\Delta m}{m}\right)^2}\right.$$
$$\left. + \left(\frac{e^{-\lambda t_c}}{1 - e^{-\lambda t_c}}\right)^2 \left[(\lambda \Delta t_c)^2 + (t_c \Delta\lambda)^2\right] + (t_d \Delta\lambda)^2 + (\lambda \Delta t_d)^2 \right] \tag{34}$$

To illustrate the treatment of the flux variation between the sample and standard, the following data and assumptions will be used:

1) Data taken from Exp 8-27-69, counts 2, 3, and 4; (two manganese standards and a magnesium oxide crystal).

2) The 1.81 Mev full energy peak of manganese-56 is used. T 1/2 = 2.576 $\pm$ 0.0005 hr, λ = 0.2690 $\pm$ 0.00005 hr.

3) Peak areas and uncertainties are given by ICPEAX.

4) Uncertainties in the counting and decay times are 0.0003 and 0.0083 hr respectively, (to be discussed later).

Using this data and these assumptions, Equation 34 gives a specific area for standard A of

$$(\bar{A} \pm \Delta\bar{A})_C = \frac{(2240)(0.2690)}{\left(1 - e^{-(0.269)(0.278)}\right)\left(e^{-(0.269)(1.20)}\right) 2.32}$$

$$\left[1 \pm \sqrt{\left(\frac{45}{2240}\right)^2 + \left(\frac{0.09}{2.32}\right)^2 + \left(\frac{0.9282}{0.0718}\right)^2 (0.00007)^2}\right.$$

$$\left. + (0.0001)^2\right) + (2 \times 10^{-5})^2 + (0.0002)^2\right]$$

$$= \frac{(2240)(0.2690)}{(0.0720)(0.968)(2.32)}\left[1 \pm \sqrt{4.0 \times 10^{-4} + 8.0 \times 10^{-5}}\right.$$

$$\left. + 2.5 \times 10^{-7} + 4 \times 10^{-10} + 4 \times 10^{-8}\right]$$

$$(\overline{A} \pm \Delta\overline{A})_C = 3730 \pm 75 \text{ counts/hr ug}$$

The specific activity of the same peak in sample C is

$$(\overline{A} \pm \Delta\overline{A})_A = \frac{(794)(0.2690)}{(0.0720)(0.477)(2.24)} \left[1 \pm \sqrt{\left(\frac{25}{794}\right)^2 + \left(\frac{0.02}{2.24}\right)^2} \right.$$

$$\overline{+ \left(\frac{0.9282}{0.0718}\right)^2 \left[(0.00007)^2 + (0.0001)^2\right] + (5.1 \times 10^{-4})^2}$$

$$\left. \overline{+ (2.2 \times 10^{-3})} \right]$$

$$= 2670 \left[1 \pm \sqrt{9.9 \times 10^{-4} + 8.0 \times 10^{-5} + 2.5 \times 10^{-7}} \right.$$

$$\left. \overline{+ 2.5 \times 10^{-7} + 4.4 \times 10^{-6}} \right]$$

$$(\overline{A} \pm \Delta\overline{A})_A = 2670 \pm 87 \text{ counts/hr ug}$$

Now applying propagation of errors theory to Equations 30 and 31, the flux ratio and its uncertainty can be written as

$$\phi_R = \frac{\phi_C}{\phi_B} = \frac{\overline{A}_C}{\overline{A}_B} = \frac{\overline{A}_C}{\overline{A}_A\left(\frac{BC}{AC}\right) + \overline{A}_C\left(\frac{AB}{AC}\right)} \tag{35}$$

$$\frac{\Delta\phi_R}{\phi_R} = \sqrt{\left(\frac{\Delta\overline{A}_C}{\overline{A}_C}\right)^2 + \frac{\left(\overline{A}_A\left(\frac{BC}{AC}\right)\right)^2\left[\left(\frac{\Delta\overline{A}_A}{\overline{A}_A}\right)^2 + \left(\frac{\Delta BC}{BC}\right)^2 + \left(\frac{\Delta AC}{AC}\right)^2\right]}{\left[\overline{A}_A\left(\frac{BC}{AC}\right) + \overline{A}_C\left(\frac{AB}{AC}\right)\right]^2}}$$

$$\overline{+ \left(\overline{A}_C\left(\frac{AB}{AC}\right)\right)^2\left[\left(\frac{\Delta\overline{A}_C}{\overline{A}_C}\right)^2 + \left(\frac{\Delta AB}{AB}\right)^2 + \left(\frac{\Delta AC}{AC}\right)^2\right]} \tag{36}$$

$$\phi_R = \frac{3730}{2670\left(\frac{0.5}{3.9}\right) + 3730\left(\frac{3.4}{3.9}\right)} = \frac{3730}{3600}$$

$$\phi_R = 1.0$$

$$\frac{\Delta\phi_R}{\phi_R} = \sqrt{\left(\frac{75}{3730}\right)^2 + \frac{\left((2670)\left(\frac{0.5}{3.9}\right)\right)^2\left[\left(\frac{87}{2670}\right)^2 + \left(\frac{0.05}{0.5}\right)^2 + \left(\frac{0.05}{3.9}\right)^2\right]}{\left[2670\frac{(0.5)}{(3.9)} + 3730\frac{3.4}{3.9}\right]^2}}$$

$$+ \left((3730)\frac{(3.4)}{(3.9)}\right)^2\left[\left(\frac{75}{3730}\right)^2 + \left(\frac{0.05}{3.4}\right)^2 + \left(\frac{0.05}{3.9}\right)^2\right]$$

$$\frac{\Delta\phi_R}{\phi_R} = \sqrt{0.001 + \frac{(1.1 \times 10^5)\left[0.0001 + 0.01 + 0.0002\right]}{1.3 \times 10^7}}$$

$$+ (1.1 \times 10^7)\left[0.001 + .0002 + .0002\right]$$

$$\frac{\Delta\phi_R}{\phi_R} = \sqrt{0.002} = 0.045$$

$$\Delta\phi_R = (1.0)(0.045)$$

$$\Delta\phi_R = 0.045$$

$$\phi_R \pm \Delta\phi_R = 1.0 \pm 0.05$$

The above development points out that the largest contribution to the uncertainty in the flux ratio, ϕ_R, arises due to the uncertainty in the measurement of the area under the full-energy peaks and to the uncertainty in the measurement of the position of the samples during irradiation.

Another factor which may introduce uncertainty is self-shielding. The self-shielding factor is defined as the limit of the ratio of the specific activity of the sample to its specific activity as its mass approaches zero. Nisle (35) approximates the self-shielding factor $f(v)$ as follows

$$f(v) = \frac{(1 - e^{-v})}{v} \tag{37}$$

where

$$v = \frac{4V\Sigma}{S}$$

and

V = sample volume,

S = sample surface,

Σ = total macroscopic cross section.

The magnesium oxide crystals used were in the form of rectangular solids 0.38 x 0.38 x 0.74 cm on a side. Since they were better than 99.9% pure, only the magnesium oxide in the matrix is considered. It has a macroscopic cross section of 0.0027 cm^{-1} (21). Using the above dimensions the sample volume is

$$V = (0.38)(0.38)(0.74) \text{ cm}^3$$

$$V = 0.107 \text{ cm}^3$$

while the surface area of the sample is

$$A = (0.38)(0.38)(2) + (0.38)(0.74)(4)$$

$$A = 1.42 \text{ cm}^2$$

so that

$$v = \frac{4V\Sigma}{S} = \frac{(4)(0.107)(0.0027)}{1.42} = 8.15 \times 10^{-4}$$

and

$$f(v) = \frac{(1 - e^{-v})}{v} = \frac{1 - e^{-8.15 \times 10^{-4}}}{8.15 \times 10^{-4}}$$

$$f(v) = 1.0$$

This demonstrates that self-shielding for the MgO crystal is negligible. Since the comparitor standards represent only approximately 1 ug of each of the several impurities present in the crystal, and because the material is spread over the surface of the capsule bottom, the self-shielding factor of the standards departs even less from unity than it does for the crystal. Therefore, the self-shielding factor in this analysis was judged to be 1.0 and assigned an uncertainty of zero.

One of the more obvious sources of error in any experiment dealing with radiation counting is the counting geometry. Counting is often done at a fixed position on a sample holder

which is at a fixed distance from the detector. This creates
an identical counting geometry providing the samples are
identical. In this work the samples were not identical.
The standards consisted of a dried solution on the bottom,
with an unknown portion extending up the sides, of the
irradiation capsule, while the MgO sample was in the form
of a rectangular solid in the bottom of a similar capsule.
This situation created an uncertainty in the source-to-
detector distance which was removed by rotating the sample
as discussed in Chapter III. Any spacial variations not
removed by this technique were judged to be small and were
ignored.

It is possible that a systematic error or uncertainty
may be introduced in the counting time by the automatic
timer associated with the analyzer. This is especially
true if the analyzer is operating with high "dead" time.
Since all counting used in the quantitative analysis was at
zero "dead" time, and since it will be shown that the uncer-
tainty in the counting time is not significant; it was
assigned a conservative value of $\pm$ 1 sec for this example.

The uncertainty in the decay time, or time since
irradiation, is somewhat greater for several reasons. First,
the time of the end of the irradiation was read by the
reactor operator introducing several seconds of uncertainty.
Second, the clock used to read the time of the end of

irradiation is not the same clock as used to read the decay times, and third, the decay times are read by the experimenter introducing another uncertainty. Because, as will be shown, the uncertainty in the decay time is not a significant factor in the overall uncertainty, a conservative value of $\pm$ 30 sec was assigned to the decay time uncertainty.

An uncertainty related to the counting and decay time is the uncertainty in the half-life. For this work the half-life values tabulated in Lederer, Hollander, and Perlman (28) are used. The uncertainty is considered to be $\pm$ one-half of the last significant figure.

The determination of the area of the full-energy peak produces an uncertainty which is a function of the count rate, the number of accumulated counts, the background count, and the presence of adjacent full-energy peaks. The area and the uncertainty in the area used in this work was obtained from the data by a computer program ICPEAX (Appendix A). It was empirically verified that the areas given by this program gave more consistent results than the results of "hand" calculations discussed in Chapter II.

Applying the propagation of errors theory as given in Chapter II to the manganese example reveals the relative contribution of each of the uncertainties discussed above. Ignoring the self-shielding and counting geometry factors

for the reasons discussed, Equation 16 becomes

$$(m \overset{+}{_-} \Delta m)_u = m_S A_R \emptyset_R D_R C_R \left[1 \overset{+}{_-} \sqrt{\left(\frac{\Delta m_S}{m_S}\right)^2 + \left(\frac{\Delta A_R}{A_R}\right)^2 + \left(\frac{\Delta \emptyset_R}{\emptyset_R}\right)^2 + \left(\frac{\Delta D_R}{D_R}\right)^2 + \left(\frac{\Delta C_R}{C_R}\right)^2} \right]$$

(38)

The mass of the manganese standard as computed earlier in this chapter is

$$(m \overset{+}{_-} \Delta m)_S = (2.32 \overset{+}{_-} 0.02) \times 10^{-6} \text{ gm}$$

The peak area ratio between the unknown, A_u, and the standard, A_S, is given as

$$(A \overset{+}{_-} \Delta A)_R = \frac{A_u}{A_S} \left[1 \overset{+}{_-} \sqrt{\left(\frac{\Delta A_u}{A_u}\right)^2 + \left(\frac{\Delta A_S}{A_S}\right)^2} \right]$$

(39)

Inserting the peak areas and uncertainties as provided by ICPEAX, Equation 39 yields

$$(A \overset{+}{_-} \Delta A)_R = \frac{4489}{2245} \left[1 \overset{+}{_-} \sqrt{\left(\frac{95}{4489}\right)^2 + \left(\frac{45}{2245}\right)^2} \right]$$

$$(A \overset{+}{_-} \Delta A)_R = 1.990 \left[1 \overset{+}{_-} \sqrt{4.5 \times 10^{-4} + 4 \times 10^{-4}} \right]$$

$$(A \overset{+}{_-} \Delta A)_R = 1.990 \overset{+}{_-} 0.058$$

The ratio of the decay of the standard to that of the unknown is given as

$$(D \pm \Delta D)_R = \frac{e^{-\lambda t_{d_s}}}{e^{-\lambda t_{d_u}}}\left[1 \pm \sqrt{(\lambda_\Delta t_{d_s})^2 + (t_{d_s}\Delta\lambda)^2 + (\lambda_\Delta t_{d_u})^2 + (t_{d_u}\Delta\lambda)^2} \right] \tag{40}$$

where

$$T_{\frac{1}{2}} = 2.576 \pm 0.0005 \text{ hrs}$$

and

$$\lambda = \frac{0.69315}{(2.576)} = (0.2690 \pm 0.0001) \frac{1}{\text{hr}}$$

so that

$$(D \pm \Delta D)_R = \frac{e^{-0.269(1.2)}}{e^{-0.269(1.5)}}\left[1 \pm \sqrt{(0.269)(0.0083)^2 + (120)(0.0001)^2 + (0.269)(0.0083)^2 + (1.5)(0.0001)^2} \right]$$

$$(D \pm \Delta D)_R = \frac{0.726}{0.660} \quad 1 \pm \sqrt{4.6 \times 10^{-6} + 3.6 \times 10^{-5} + 4.6 \times 10^{-6} + 5.6 \times 10^{-6}}$$

$$(D \pm \Delta D)_R = 1.101 \pm 0.001$$

The ratio of the counting time of the standard to that of the unknown is given as

$$(c \overset{+}{_-} \Delta c)_R = \frac{\frac{(1 - e^{-\lambda t_{c_s}})}{(1 - e^{-\lambda t_{c_u}})} \left[1 \overset{+}{_-} \sqrt{\left(\frac{e^{-\lambda t_{c_s}}}{1 - e^{-\lambda t_{c_s}}} \right)^2 \frac{\left[\left(t_{c_s} \Delta \lambda_s \right)^2 + \left(\lambda \Delta t_{c_s} \right)^2 \right] + \left(\frac{e^{-\lambda t_{c_u}}}{1 - e^{-\lambda t_{c_u}}} \right)^2}{\left[\left(t_{c_u} \Delta \lambda \right)^2 + \left(\lambda \Delta t_{c_u} \right)^2 \right]}} \right]$$

(41)

here

$$t_{s_c} \overset{+}{_-} \Delta t_{s_c} = 1000 \overset{+}{_-} 1 \text{ sec} = 0.2780 \overset{+}{_-} 0.0003 \text{ hrs}$$

$$t_{c_u} \overset{+}{_-} \Delta t_{c_u} = 4000 \overset{+}{_-} 1 \text{ sec} = 1.11 \overset{+}{_-} 0.0003 \text{ hrs}$$

$$(c \overset{+}{_-} \Delta c)_R = \frac{0.0720}{0.2580} \left[1 \overset{+}{_-} \sqrt{\left(\frac{0.9280}{0.072} \right)^2 \frac{\left[((0.278)(0.0001))^2 + ((0.269)(0.0003))^2 \right] + \left(\frac{0.742}{0.258} \right)^2}{\left[((1.11)(0.0001))^2 + ((0.269)(0.0003))^2 \right]}} \right]$$

$$(c \overset{+}{_-} \Delta c)_R = 0.2790 \left[1 \overset{+}{_-} \sqrt{(16.5) \left[6.9 \times 10^{-9} + 6.5 \times ^{-9} \right] + (8.6) \left[1.11 \times 10^{-9} + 6.5 \times 10^{-9} \right]} \right]$$

$$(c \overset{+}{_-} \Delta c)_R = 0.2790 \overset{+}{_-} 0.0001$$

Putting all of the factors calculated above into

$$(m \pm \Delta m)_u = m_S A_R \emptyset_R D_R C_R \left[1 \pm \sqrt{ \left(\frac{\Delta m_S}{m_S}\right)^2 + \left(\frac{\Delta A_R}{A_R}\right)^2 + \left(\frac{\Delta \emptyset_R}{\emptyset_R}\right)^2 + \left(\frac{\Delta D_R}{D_R}\right)^2 + \left(\frac{\Delta C_R}{C_R}\right)^2 } \right] \quad (42)$$

yields the mass and the uncertainty in the mass of the unknown.

$$(m \pm \Delta m)_u = (2.32)(1.990)(1.0)(1.101)(0.2790) \left[1 \pm \sqrt{ \left(\frac{0.025}{2.32}\right)^2 + \left(\frac{0.058}{1.990}\right)^2 + \left(\frac{0.045}{1.0}\right)^2 + \left(\frac{0.001}{1.101}\right)^2 + \left(\frac{0.0001}{0.2790}\right)^2 } \right]$$

$$(m \pm \Delta m)_u = 1.4 \left[1 \pm \sqrt{1.15 \times 10^{-4} + 8.5 \times 10^{-4} + 2.0 \times 10^{-3} + 1.0 \times 10^{-6} + 1.28 \times 10^{-5}} \right]$$

$$(m \pm \Delta m)_u = 1.4 \pm 0.1 \text{ ug}$$

To find the concentration in ppm, the mass of the impurity is divided by the mass of the crystal.

$$ppm \pm \Delta ppm = \frac{m_u}{m_S} \left[1 \pm \sqrt{ \left(\frac{\Delta m_u}{m_u}\right)^2 + \left(\frac{\Delta m_c}{m_c}\right)^2 } \right] \quad (43)$$

$$= \frac{1.4}{0.243} \left[1 \pm \sqrt{ \left(\frac{0.1}{1.4}\right)^2 + \left(\frac{0.0001}{0.243}\right)^2 } \right]$$

$$= 5.9 \left[1 \overset{+}{\underset{-}{}} \sqrt{2.1 \times 10^{-3} + 1.7 \times 10^{-7}} \right]$$

$$\text{ppm} \overset{+}{\underset{-}{}} \Delta\text{ppm} = 5.9 \overset{+}{\underset{-}{}} 0.3$$

Equations 42 and 43 show that the largest uncertainties in order of decreasing size are in the determination of the flux ratio, the peak area ratio, and the mass of the standard. The uncertainty in the determination of the flux ratio, which is about ten times larger than the other two, has been shown to be comprised of two things:

1) A contribution from the uncertainty in the location of the two flux calibration standards with respect to the magnesium oxide crystal;

2) A contribution from the uncertainty in the full-energy peak areas.

The operational characteristics associated with a particular detector, analyzer, and data handling system are also possible sources of error which are hard to evaluate. Since the same system was used for each associated pair of experiments, each of which is complete in itself, this error is assumed to cancel. Since there was no evidence that this uncertainty should be considered, it was neglected.

Summarizing the error analysis, it appears that the largest sources of uncertainty in the qualitative analysis are interfering full-energy peaks at approximately the same

energies, peaks too small to be statistically significant, improper calibration and contamination prior to irradiation. The chances for error are increased as the sensitivity limit is approached. Quantitatively, the largest sources of uncertainty listed in descending order are in the determination of the flux ratio between the sample and standard, the full-energy peak area, and the mass of the standard. Since about half of the uncertainty in the flux ratio comes from the uncertainty in the peak areas used, improvement in this factor will do much to improve the accuracy of the quantitative analysis. Another suggestion is to rotate the samples about one another during irradiation exposing both to the same flux and eliminating the uncertainty in the flux ratio altogether.

Three recommendations for further study are:

1) Develop a more accurate method of determining the full-energy peak areas.

2) Eliminate the flux gradient by rotating the sample during irradiation or by some other technique.

3) Develop a technique for the analysis of the calcium, a common impurity in magnesium oxide, and other short lived activities.

CHAPTER VII. SUMMARY

A technique for the qualitative and quantitative non-destructive analysis of a solid magnesium oxide specimen has been developed. The ability to quantitatively determine trace impurities in the ppb range using specimens in an "as is" form has been shown.

The technique utilizes neutron activation and gamma ray spectrometry to detect impurities whose half-lives are greater than one hour. Comparitor techniques are used for the quantitative analysis and have been shown to give an accuracy of $\pm$ 5%. A detailed error analysis is given.

A comparison of the value of the Ge(Li) versus the NaI(Tl) detector system and between the qualitative results using activation analysis and emission spectroscopy is made.

The technique as developed has two obvious shortcomings. First, isotopes whose activities have half-lives on the same order of magnitude as the magnesium matrix could not be detected and second, the technique is time consuming. A minimum of four weeks must be allowed for a complete qualitative and quantitative analysis.

BIBLIOGRAPHY

1. Abu-Samra, A. Analysis of a Damascus steel by neutron and gamma activation. Unpublished M.S. thesis. Ames, Iowa, Library, Iowa State University of Science and Technology. 1965.

2. Anders, Oswald U. Instrumental neutron activation analysis using TRIGA reactor high-resolution gamma spectrometer and computer. Analytical Chemistry 41: 428-437. 1969.

3. Anders, O. U. and Beamer, W. H. Resolution of time-dependent gamma spectra with a digital computer and its use in activation analysis. Analytical Chemistry 33: 226-230. 1961.

4. Baumann, N. P. and Stroud, M. B. Self-shielding of detector foils in reactor fluxes. Nucleonics 23, No. 8: 98-100. 1965.

5. Bell, Howard. Creep in ceramic materials. Iowa State University Project Themis Ceramic Materials Progress Report 7: 6-9. 1969.

6. Burrus, Walter R. and Bogert, Dixon. A study of the errors associated with spectral analysis methods. Gatlinburg, Tennessee Symposium Proceedings 1962: 127-137. 1963.

7. Cali, J. P., Weiner, J. R., and Rocco, G. G. The accuracy of radioactivation analysis. International Conference on Modern Trends in Activation Analysis Proceedings 1965: 253-259. 1965.

8. Cilindro, Leodegario de Gracia. Neutron activation analysis for iridium, palladium, and silver in platinum. Unpublished Ph.D. thesis. Ames, Iowa, Library, Iowa State University. 1967.

9. Covell, D. F. A new method of determining photopeak areas. Analytical Chemistry 31: 1785. 1959.

10. Currie, Lloyd A. Limits for qualitative detection and quantitative determination. Analytical Chemistry 40: 586-593. 1968.

11. De Neve, R., De Soete, D., and Hoste, J. Nondestruc-
     tive activation analysis of trace impurities in
     germanium. Analytica Chimica Acta 40: 379-386. 1968.

12. Drew, D. D., Fite, L. E., and Wainerdi, R. E. Computer
     coupled activation analysis. Gatlinburg, Tennessee
     Symposium Proceedings 1962: 237-243. 1963.

13. Emergy, J. F., Dyer, F. F., Alexander, T., and Schon-
     feld, E. The evaluation of computer programs for
     gamma-ray spectrometry in activation analysis. Interna-
     tional Conference on Modern Trends in Activation
     Analysis Proceedings 1965: 212-216. 1965.

14. Fairstein, E. and Hahn, J. Nuclear pulse amplifiers-
     fundamentals and design practice. Mt. Prospect,
     Illinois, Contemporary Science, Inc. 1966.

15. Friedlander, G., Kennedy, J. W., and Miller, J. M.
     Nuclear and radiochemistry. 2nd edition. New York,
     New York, John Wiley and Sons, Inc. 1955.

16. Gilat, J. and Gurfinkel, Y. Shielding in activation
     analysis. Nucleonics 21, No. 8: 143-144. Aug. 1963.

17. Hahn, Paul Balser. Activation analysis for trace
     quantities of iodine in biological materials. Un-
     published M.S. thesis. Ames, Iowa, Library, Iowa State
     University. 1967.

18. Heath, R. L. Scintillation spectrometry, gamma-ray
     spectrum catalogue. 2nd edition. U.S. Atomic Energy
     Commission Report IDO-16880 (Idaho Operations Office,
     AEC). 1964.

19. Hunt, Lee Philip. Neutron activation analysis of
     trace rare earths in holmium oxide. Unpublished Ph.D.
     thesis. Ames, Iowa, Library, Iowa State University.
     1967.

20. Jones, John Taylor. The diffusion of manganese oxide
     in single crystals of periclase. Unpublished Ph.D.
     thesis. Salt Lake City, Utah, Library, University of
     Utah. 1965.

21. Kaplan, I. Nuclear physics. 2nd edition. Reading,
     Massachusetts, Addison-Wesley Publishing Co., Inc.
     1962.

22. Kenna, B. T. and Conrad, F. J. Determination of sodium in high purity silica by activation analysis. Talanta 15: 418-420. 1968.

23. Kenna, B. T. and Van Domelsen, B. N. Neutron activation: relationship of sample mass to self-shielding factor. International Journal of Applied Radiation and Isotopes 17: 47-50. 1966.

24. Koch, R. C. Activation analysis handbook. New York, New York, Academic Press, Inc. 1960.

25. Korthoven, Peter J. M., Wechter, Margaret A., and Voigt, Adolf F. Determination of gadolinium and europium in their tungsten bronzes by high energy photon activation and computer resolution of gamma-ray spectra. Analytical Chemistry 39: 1594-1598. 1967.

26. Lab Glass Inc. Lab Glass: catalogue. Lab Glass Inc., Vineland, New Jersey. 1969.

27. Leddecotte, G. W. Experience in the U.S.A. on the use of radioactivation analysis. 1960. Original not available; cited in Payne, Bryan R. Radioactivation Analysis Symposium Proceedings 1959: 62. 1960.

28. Lederer, C. M., Hollander, J. M., and Perlman I. Table of isotopes. 6th edition. New York, New York, John Wiley and Sons, Inc. 1967.

29. Lee, Bong Kyu. Neutron activation analysis applied to arsenic determination. Unpublished Ph.D. thesis. Ames, Iowa, Library, Iowa State University. 1968.

30. Lee, Hee Myong. Determination of impurities in single crystals of magnesium oxide by neutron activation analysis. Analytica Chimica Acta 41: 431-440. 1968.

31. Lenihan, J. M. A. and Thomson, S. J., editors. Activation analysis, principles and applications. New York, New York, Academic Press, Inc. 1965.

32. Lewis, W. B. How to choose irradiation time. Nucleonics 12, No. 10: 30-33. 1954.

33. Meinke, Wayne W. and Shideler, Ronald W. Activation analysis: new generators and techniques make it routine. Nucleonics 20, No. 3: 60-65. 1962.

34. Moses, Alfred J. Nuclear Techniques in Analitical Chemistry. New York, New York, Permagon Press, Inc. 1964.

35. Nisle, Robert G. Neutron-absorption alignment chart. Nucleonics 18, No. 3: 86-87. March 1960.

36. Nuclear Diodes, Inc. The selection and use of Ge(Li) detectors. Nuclear Diodes, Inc., Prairie View, Illinois. 1968.

37. Op De Beeck, J. and Hoste, J. The simultaneous determination of silver, gold, and mercury in high-purity lead by neutron activation analysis. Analytical Chimica Acta 35: 427-440. 1966.

38. Price, William J. Nuclear radiation detection. 2nd edition. New York, New York, McGraw-Hill Book Co., Inc. 1964.

39. Priest, H. F., Burns, F. C., and Priest, G. L. Neutron flux distribution from a 14 Mev neutron generator. Nuclear Instruments and Methods 50: 141-146. 1967.

40. Prussin, S. G., Harris, J. A., and Hollander, J. M. Application of lithium-drifted germanium gamma-ray detectors to neutron activation analysis: nondestructive analysis of aluminum. International Conference on Modern Trends in Activation Analysis Proceedings 1965: 357-363. 1965.

41. Robinson, E. L., Furr, A. K., and Robins, C. H. A spectrum stripping technique for qualitative activation analysis using monoenergetic gamma spectra. Nuclear Instruments and Methods 63: 205-209. 1968.

42. Ruzicka, Jaromir and Stary, Jiri. Substoichiometry in radiochemical analysis. Glasgow, Great Britain, Pergamon Press Ltd. 1968.

43. Salmon, L. Analysis of gamma-ray scintillation spectra by the method of least squares. Nuclear Instruments and Methods 14: 193-199. 1961.

44. Schonfeld, E. Alpha-A computer program for the determination of radioisotopes by least-squares resolution of the gamma-ray spectra. Nuclear Instruments and Methods 42: 213-218. 1966.

45. Siegbahn, Kai, editor. Alpha-, beta-, and gamma-ray spectroscopy. Amsterdam, Holland, North Holland Publishing Co. 1965.

46. Tera, Fouad, Ruch R. R., and Morrison, G. H. Preconcentration of trace elements by precipitation ion exchange. Analytical Chemistry 37: 358-360. 1965.

47. Trombke, J. I. and Schmadebeck, R. L. A method for the analysis of pulse-height spectra containing gain-shift and zero-drift compensation. Nuclear Instruments and Methods 62: 253-261. 1968.

48. Voigt, A. F., Jewett, G. L., Jacobson, E. C., Malaby, K. L., and Woods, J. D. The determination of trace amounts of tantalum and tungsten in metals. International Conference on Modern Trends in Activation Analysis Proceedings 1965: 26-31. 1965.

49. Weast, Robert C., Selby, Samuel M., and Hodgman, Charles D., editors. Handbook of chemistry and physics. Cleveland, Ohio, The Chemical Rubber Co. 1964.

50. Wechter, Margaret A. and Voigt, Adolf F. Determination of potassium, rubidium, and barium in their tungsten bronzes by neutron and high energy photon activation. Analytical Chemistry 38: 1681-1683. 1966.

51. Wilhelm, H. A. Purity-grade metals available from American producers. U.S. Atomic Energy Commission Report IS-2-29 (Iowa State University, Ames, Iowa). 1967.

ACKNOWLEDGEMENTS

APPENDIX A. ICPEAX

"ICPEAX-7"[1] is a FORTRAN IV program written for the IBM
360/65 computer. It automatically detects full-energy peaks
in Ge(Li) spectra, determines the peak parameters, and can
plot the spectra. While the program was designed to be used
with the Ge(Li) detector, it also works with the NaI(Tl)
detector.

The input for "ICPEAX" is 1600 or less channels of raw
data punched on cards. The program detects full-energy peaks
by analysis of a smoothed second derivative of the spectrum.
All negative minima are considered full-energy peaks if two
conditions are met: The width of the peak must be between
3 to 15 channels, while the magnitude must be at least 0.35
times the standard deviation. After this preliminary search,
the results of which are printed, a gaussian fit is attempted
on all peaks. The full-energy peak background is approxi-
mated by a straight line subtracted before the analysis. At
this point the peaks are checked for a gaussian fit using
essentially the program written by Heath (18). The peaks
are considered real only if they satisfy the gaussian fit
routine.

The program uses the coefficients of the linear and
quadratic calibration lines of the detector to assign

---

[1]Haustein, Peter, Ames Lab, Ames, Iowa. ICPEAX-7.
Private communication. 1969.

energies to each of the peaks it considers real. The following information about each real peak is printed: location (Kev), standard deviation, width, height, area, standard deviation of the area, line slope, line intercept, fit, and the energy (using both linear and quadratic calibrations). In addition, the program will yield either a log or linear plot of the spectrum on which each of the peaks is labeled with its appropriate energy (quadratic calibration).

APPENDIX B.   PRESTO

"PRESTO"[1] is a FORTRAN IV program written for the IBM 360/65 computer which converts data in the form of IBM 7-track magnetic tape to punched card format and/or listed data on the computer output.   Data in the form of punched paper tape from the multichannel analyzer system is first recorded onto magnetic tape.   This tape is then submitted to the computer with the program to obtain listings and decks of the data.   The program was originally written for 1600 channel spectra but has been modified to accept 256, 512, and 1024 channel spectra.   Now, as before, the program will accept any number of such spectra.   For each data set either listings, card decks, or both may be obtained from the program.   If errors occur during the transfer of the data from tape to cards or listings, the program indicates the type of error on the computer output.

---

[1]Haustein, Peter, Ames Lab, Ames, Iowa.   PRESTO. Private communication.   1969.

APPENDIX C.   ELEMENTS AND REAGENTS

Specifications of Elements and Reagents
Used as Standards

1.   Ammonium Hydroxide (NH_4OH)

Manufacturer. . .Allied Chemical Corporation

Analysis. . . . .Material

Material	%
Cl	0.00005
PO_4	0.00004
SO_4	0.0001
Pb	0.00005
Fe	0.000010

2.   Antimony (Sb)

Form. . . . . . .Sb_2O_3

Manufacturer. . .Baker Chemical Company

Analysis. . . . .Material

Material	%
Sb_2O_3	99.7
SO_4	0.01
As	0.10
Cl	0.015
Heavy Metal (Pb)	0.001
Fe	0.01

3.   Barium (Ba)

Form. . . . . . .BaO_2

Manufacturer. . .Allied Chemical Corporation

Analysis.....Material	%
Fe	0.03
Pb	0.002
Cl	0.01
Ca	1.0

4. Calcium (Ca)

Form.......CaO

Manufacturer...Mallinckrodt Chemical Works

Analysis.....Material	%
Pb	0.01
Cl	0.005
Fe	0.10
Mg	1.0
NO_3	0.05
SO_4	0.1

5. Cesium (Cs)

Form.......$CsNO_3$

Source......Ames Lab

Analysis.....no specifications given

6. Chromium (Cr)

Form.......CrO_3

Manufacturer...Baker Chemical Company

Analysis.....Material	%
CrO_3	99.1
Insolubles	0.005

Material	%
Cl	0.003
NO_3	0.050
SO_4	0.003
Na	0.004
Fe, Al, Ba	0.015

7. Cobalt (Co)

Form. . . . . . .metal foil

Source. . . . . .Ames Lab

Analysis. . . . .purity grade

8. Copper (Cu)

Form. . . . . . .CuO (powder)

Manufacturer. . .Baker Chemical Company

Analysis. . . . .

Material	%
Insolubles	0.01
Cl	0.005
NO_3	0.001
SO_4	0.01
Fe	0.06

9. Glacial Acetic Acid (CH_3COOH)

Manufacturer. . .Dupont Chemical Company

Analysis. . . . .

Material	%
Cl	0.00005
SO_4	0.00005
Fe	0.00002
Heavy Metal (Pb)	0.00005

10. Hydrofluoric Acid (HF)

    Manufacturer. . .Mallinckrodt Chemical Works

    Analysis. . . . .

Material	%
As	0.000005
Cl	0.0005
H_2SiF_6	0.01
Heavy Metal (Pb)	0.00005
Fe	0.0001
PO_4	0.0001
SO_4	0.0001
SO_3	0.001

11. Hydrogen Peroxide (H_2O_2)

    Manufacturer. . .Baker Chemical Company

    Analysis. . . . .

Material	%
H_2O_2	30
Cl	0.0003
N	0.0008
PO_4	0.010
Pb	0.00005
Fe	0.00001
Cu	0.00002
Ni	0.00002

12. Iron (Fe)

    Form. . . . . . .metal

    Source. . . . . .Ames Lab

    Analysis. . . . .purity grade

13. Manganese (Mn)

Form. . . . . . .MnO_2

Manufacturer. . .Mallinckrodt Chemical Works

Analysis. . . . .Material

Material	%
MnO_2	99.5
Alkalis and Earths	0.2
Cl	0.01
Insolubles	0.05
NO_3	0.05
SO_4	0.05

14. Molybdenum Trioxide (MoO_3)

Manufacturer. . .Baker Chemical Company

Analysis. . . . .Material

Material	%
MoO_3	99.5
Insolubles	0.002
Cl	0.001
NO_3	0.003
PO_4	0.0002
SO_4	0.01
NH_4	0.008
Pb	0.002

15. Nickel (Ni)

Form. . . . . . .$NiSO_4$

Manufacturer. . .Baker Chemical Company

Analysis. . . . .Material   %

                              Insolubles   0.003

                              Cl 0.0003

                              NO_3 0.005

                              Pb 0.001

                              Cu 0.001

                              Co 0.06

                              Fe 0.001

                              Alkalis and Earths   0.20

16.   Nitric Acid (HNO_3)

      Manufacturer. . .Baker Chemical Company

      Analysis. . . . .Material   %

                              HNO_3 70.0-71

                              Cl 0.000008

                              SO_4 0.00008

                              As 0.0000005

                              Pb 0.00001

                              Fe 0.00001

                              Cr 0.00001

                              PO_4 0.00002

                              Cu 0.000005

                              Ni 0.000005

17.   Phosphoric Acid

      Manufacturer. . .Baker Chemical Company

      Analysis. . . . .None given

18. Scandium (Sc)

    Form. . . . . . .metal

    Source. . . . . .Ames Lab

    Analysis. . . . .purity grade

19. Sulfuric Acid

    Manufacturer. . .Baker Chemical Company

    Analysis. . . . .

Material	%
Cl	0.00001
NO_3	0.00005
NH_4	0.0001
SO_4	0.0001
As	0.00001
Pb	0.0001
Fe	0.00001
Cu	0.00005
Ni	0.00005

20. Titanium (Ti)

    Form. . . . . . .TiO_2

    Manufacturer. . .Matheson, Coleman, and Bell, Inc.

    Analysis. . . . .

Material	%
As	0.0002
Fe	0.01
Pb	0.02
Zn	0.01

APPENDIX D. EXPERIMENTAL EQUIPMENT

Make, Model, and Serial Number
of the Experimental Equipment

Description	Make	Model no.	Serial no.
Output typewriter and paper tape punch	Teletype	33TC	129743
Teletype drive	Nuclear Data	-	67-33
Master control	Nuclear Data	2200	67-168
Analog to digital	Nuclear Data	2200	67-232
Tape transport	Nuclear Data	-	67-14
Reduce/integrate unit	Nuclear Data	-	67-4
Memory	Nuclear Data	-	67-141
Oscilloscope	Hewlett Packard	H77-120B	601-11140
High voltage power supply	Nuclear Data	537	67-39
Preamp, amp, and discriminator	Nuclear Data	520	66-204
Preamp	ORTEC	118A	625S
Amplifier	ORTEC	435	82
Ge(Li) detector	ORTEC	8201-0335	9-P421
NaI(Tl) detector	Harshaw	12S12	DE354
AEC bin and power supply	Nuclear Data	510	711150
6V power supply	Nuclear Data	-	67-147

Description	Make	Model no.	Serial no.
High voltage power supply	Fluke	405B	1692
Electrometer and 1000:1 probe	Keithley Instruments	610B	34819